Zinc- and cadmium-isotope evidence for redox-driven perturbations to global micronutrient cycles during Oceanic Anoxic Event 2 (Late Cretaceous)

Tim C. Sweere[1,2], Alexander J. Dickson[1,3], Hugh C. Jenkyns[1], Don Porcelli[1], Gideon M. Henderson[1]

1. Department of Earth Sciences, University of Oxford, South Parks Road, Oxford, OX1 3AN, UK
2. Institute of Geochemistry and Petrology, Department of Earth Sciences, ETH Zürich, Clausiusstrasse 25, 8092 Zürich, Switzerland, tim.sweere@erdw.ethz.ch
3. Department of Earth Sciences, Royal Holloway University of London, Egham, Surrey, TW20 0EX, UK

Abstract

This study uses organic-rich sediments from the Tarfaya Basin, Morocco, to assess the Cd- and Zn-isotope response to dramatic global palaeoenvironmental change during the Cenomanian–Turonian interval (Late Cretaceous). These organic-rich continental-margin deposits include an expression of Oceanic Anoxic Event 2 (OAE 2, ~94 Ma), an interval associated with the spread of low-oxygen marine environments and widespread burial of organic-rich sediments. Due to placement of the Tarfaya Basin in a region of upwelling and relatively constant local environmental conditions, the stratigraphic variations in δ^{114}Cd and δ^{66}Zn values largely reflect changes in the seawater isotopic composition of the sub-surface proto-North Atlantic Ocean. Positive shifts of ~0.2–0.3 ‰ away from background values in δ^{114}Cd and δ^{66}Zn are observed during the main phase of the positive carbon-isotope excursion associated with OAE 2. These isotopic shifts are coeval with decreases in Cd/TOC and Zn/TOC ratios and thus imply that drawdown of isotopically light Cd and Zn from seawater inventories was a result of extensive burial of these metals in organic-rich marine sediments globally. Low δ^{66}Zn values during the Plenus Cold Event, a cooler episode during OAE 2, are similar in timing and magnitude to variations found in the English Chalk (Eastbourne, UK) and support the inference of a global control on these isotopic excursions. The δ^{66}Zn values during the Plenus Cold Event are taken to record global oxygenation, possibly including the remobilization of isotopically light Zn from continental-margin sediments. A considerably smaller change in δ^{114}Cd values for this interval implies that the Cd- and Zn-isotope systems can provide information about slightly different environmental processes, with global seawater composition with respect to Zn also being influenced by the magnitude of oxic removal sinks and isotopically light Zn input fluxes from sediments and hydrothermal fluids.

1. Introduction

Continental margins are important repositories for organic carbon in the modern ocean and are hotspots of ocean deoxygenation (e.g. Muller-Karger et al., 2005). These features are particularly pronounced in low-latitude sites of upwelling where Oxygen Minimum Zones (OMZs) develop with high rates of organic-carbon burial occurring in response to enhanced primary productivity. The immobilization of many redox-dependent, bio-active trace metals such as Cd, Zn and Mo at these depositional settings can have significant impact on the global cycles of these metals (e.g. Brumsack, 2006; Scholz, 2018). Organic-rich continental-margin sediments also represent a possibly important archive for the reconstruction of global metal budgets associated with past global environmental change. Here, Cd- and Zn-isotope analyses of organic-rich continental-margin sediments are used to evaluate the impact of global environmental change on the mass balance of these elements in Late Cretaceous time.

1.1. Oceanic Anoxic Event 2

The widespread deposition of organic-rich sediments during a number of intervals in the Mesozoic Era has been associated with global warming, the spread of low-oxygen marine environments, and other perturbations to ocean chemistry (e.g. Jenkyns, 2010; Dickson, 2017, O'Brien et al., 2017). One of the most severe and best-studied examples of these events is the Cenomanian–Turonian (Late Cretaceous, ~94 Ma) Oceanic Anoxic Event 2 (OAE 2) (Schlanger and Jenkyns, 1976; Arthur et al., 1990). To drive and sustain the high export productivity rates needed to reproduce the oceanic redox change associated with this event, geochemical models require a high availability of nutrients in the surface ocean for timescales on the order of 10^5 years (Monteiro et al., 2012). The availability of the major nutrients phosphorus and nitrogen can be explained by their behaviour under anoxic conditions. Phosphorus can be regenerated from anoxic sediments, while the increased fixation of atmospherically derived N_2 by cyanobacteria acts to increase bio-available nitrogen (e.g. Kuypers et al., 2004; Mort et al., 2007; Kraal et al., 2010; Monteiro et al., 2012). The overarching positive carbon-isotope excursion that reflects globally enhanced marine organic-matter burial is conventionally taken to define OAE 2 and can be used as a correlative tool (e.g. Schlanger & Jenkyns, 1976; Arthur et al., 1990; Tsikos et al., 2004). Subdivisions of the carbon-isotope excursion include the Plenus Cold Event interval (section 1.1.1) and the so-called plateau phase that features high and relatively stable $\delta^{13}C$ values reflecting peak-organic carbon burial conditions globally (Figure 2).

Cd and Zn are bio-active trace elements, with at least the latter involved in a number of critical enzymes required for marine life, and both show strong nutrient-like behaviour in the modern ocean (e.g. Bruland, 1980; Morel et al., 1994). Both these elements have a strong affinity for sulfides and are therefore removed from the ocean when reducing conditions increase the formation of such compounds (e.g. Little et al., 2015). Previous studies have suggested that there were decreases in redox-sensitive or chalcophilic trace-element concentrations in seawater during OAE 2 in response to the spread of reducing environments (van Bentum et al., 2009; Hetzel et al., 2009; Owens et al., 2016; Dickson et al., 2016, 2017). However, the magnitude and geographical extent of trace-metal drawdown is difficult to assess from sediment concentration data, due to strong redox controls on their burial in the local environment. Cd- and Zn-isotope ratios offer a complementary way to quantify the behaviour of these important bioactive elements during major environmental perturbations such as OAE 2, because changes in the global mass balance will affect the seawater isotopic composition (e.g. John et al., 2017; Isson et al., 2018).

1.1.1 The Plenus Cold Event

Environmental conditions were not uniform during OAE 2. The Plenus Cold Event represents a period of intra-OAE cooling and was associated with major changes to ocean chemistry (Gale & Christensen, 1996; Forster et al., 2007; Sinninghe Damsté et al., 2010; van Helmond et al., 2014, 2016; Jenkyns et al., 2017; Gale et al., 2019; O'Connor et al., 2020). This interval of cooling was associated with more oxygenated conditions, illustrated by colonization of formerly anoxic sea floors by benthonic organisms, and coincides with a slight negative excursion in the global C-isotope curve, which likely indicates a temporary drop in global organic-carbon burial rates (Tsikos et al., 2004; Jarvis et al., 2011; Jenkyns et al., 2017). Trace-element anomalies found in carbonates recording the Plenus Cold Event have been linked to reoxygenation of previously deposited organic matter and temporary loss of anoxic sinks for redox-sensitive and chalcophilic elements (Jenkyns et al., 2017). Similar anomalies in trace-element concentrations and Cr isotopes from time-equivalent sections from the Western Interior Seaway have, however, stressed mafic volcanic influence without specific attribution to the changing redox conditions (Eldrett et al., 2014; Holmden et al., 2016). Perturbations to the global Zn and U cycles during the Plenus Cold Event interval have also been inferred from seawater isotopic compositions of these elements preserved in carbonate successions: data that are consistent with generally more oxygenated conditions globally (Clarkson et al., 2018; Sweere et al., 2018).

1.2. Cd- and Zn-isotope systematics

Biological uptake of isotopically light Cd results in high δ^{114}Cd values in the modern surface ocean, whereas δ^{66}Zn values of surface waters are generally lower than in deep waters (e.g. Conway and John, 2014, 2015). For Zn, this observation is remarkable, as culture studies have generally shown the preferential uptake of isotopically light Zn by primary producers in most conditions (John et al., 2007, John and Conway, 2014, Köbberich and Vance, 2019). One explanation for this apparent discrepancy is the reversible scavenging of isotopically heavy Zn by sinking particles (John and Conway, 2014; Weber et al., 2018). Other studies have also stressed the importance of Southern Ocean Zn cycling on global patterns (Vance et al., 2017; De Souza et al., 2018; Sieber et al., 2020), whereas more recent studies show evidence for an (anthropogenic) source of isotopically light Zn to the surface ocean (Lemaitre et al., 2020). Despite these complexities, both elements are highly depleted in surface waters relative to deep waters so that, to a first approximation, phytoplankton quantitively remove the elements and therefore have a similar isotope composition to that added to the surface by upwelling and vertical diffusion. However, recent data on particulates suggests that partial remineralization in sub-surface waters may leave sinking particles isotopically lighter than dissolved Cd (Janssen et al., 2019). The isotopic composition of the deep ocean is nearly homogeneous for both elements and is set by the relative proportions of different oceanic input and output fluxes.

For Zn, the weighted mean of riverine δ^{66}Zn input to the modern ocean has a value of ~0.33 ‰, which is within the uncertainties of estimates for the bulk silicate earth composition (0.28 ± 0.05 ‰, 2 SD) and aeolian input (Chen et al., 2013; Little et al., 2014). Recent estimates for the isotopic composition of Zn inputs from continental margins (-0.51 to +0.01‰) and hydrothermal sources (~ -0.42 ‰) have considerably lower δ^{66}Zn values than riverine inputs (Lemaitre et al., 2020), but the size and global relevance of these fluxes are still debated (John et al., 2008; Conway and John, 2014; Little et al., 2014; Roshan et al., 2016). Organic-rich continental-margin sediments represent the only known sink for isotopically light Zn (Little et al., 2016). Sediments underlying the restricted, euxinic deep waters of the Black Sea and Cariaco Basin have average δ^{66}Zn values of ~0.5 ‰, identical to the average deep-ocean composition as a result of near-quantitative removal of Zn under such conditions (Vance et al., 2016; Isson et al., 2018). δ^{66}Zn values for other sinks in oxic environments (Fe-Mn oxyhydroxides, carbonates) are 0.4–0.5 ‰ higher than those of average deep ocean seawater (Pichat et al., 2003; Little et al., 2014).

The Cd cycle shows similarities to Zn as the average lithosphere (~-0.04‰), riverine (~0.24‰), aeolian (~-0.02‰) and hydrothermal (~0.06‰) inputs of Cd to the ocean all have lower δ^{114}Cd values than the dissolved deep-ocean composition (~0.3‰) (John et al., 2017 and references therein). The isotopic compositions of ocean outputs have not been characterized in great detail, apart from those of Fe-Mn oxyhydroxide crusts, which are not associated with significant isotopic fractionation and record seawater values (Schmitt et al., 2009; Horner et al., 2010). In contrast to Zn, Cd sinks that are isotopically heavier than seawater have not been recognized.

Cd and Zn outputs to organic-rich marine sediments are likely to relate to two main fluxes: organically bound metals and metal sulfides. Uptake in cellular organic carbon generally represents the main export mechanism of Cd and Zn to the sediment, where it may be buried as part of organic material or fixed as metal sulfides (Little et al., 2015; Weber et al., 2018). The formation of Cd and Zn sulfides in sulfdic pore waters or seawater is associated with the preferential incorporation of the lighter isotopes for both Cd and Zn, which may lead to isotopic fractionation between water and sediment if removal is non-quantitative (Conway and John, 2015; Little et al., 2016; Vance et al., 2016; Guinoiseau et al., 2018). However, due to the high stability of CdS and ZnS complexes (Al-Farawati and Van den Berg, 1999), sulfide precipitation for these elements may generally be expected to be quantitative in most environments. Non-quantitative sulfide formation may occur in conditions where dissolved Cd and Zn are available in excess of sulfide, for example, in redox transition zones in pore waters (Scholz and Neumann, 2007). It is unclear how relevant such conditions are for the global isotopic mass balances. Nonetheless, sulfide formation can impact the isotopic composition of the bulk sediment in various settings as it affects the relative proportion of sedimentary Cd and Zn in other sedimentary phases (John et al., 2017; Isson et al., 2018; Weber et al., 2018; Sweere et al., 2020). Of particular relevance to this study is organic material for which the metal-isotope ratios may be isotopically lighter than seawater due to non-quantitative biological uptake in the surface ocean or partial remobilization of sinking particles (John et al., 2007; John and Conway; 2014; Janssen et al., 2019).

Consequently, local redox conditions may impact the proportion of Cd and Zn removal in the form of CdS and ZnS and may thus explain differences in δ^{114}Cd and δ^{66}Zn for various modern marine sediments. Modern organic-rich continental-margin sediments accumulating underneath relatively shallow waters (~264 m) with anoxic to mildly sulfidic conditions, such as in the Peruvian Margin, feature higher sedimentary δ^{66}Zn values (δ^{66}Zn = ~0.3‰) than those from less reducing and deeper sites (δ^{66}Zn = ~0.0‰) (Little et al., 2016). A mostly sulfidic water column results in quantitative Zn removal in the restricted Black Sea and Cariaco Basin (δ^{66}Zn = ~0.5‰, Vance et al., 2016; Isson et al., 2018). Modern sediment data are not available for Cd in such detail, but the first results suggest generally similar patterns (Bryan, 2019).

2. Material and methods

2.1 The Tarfaya Basin

Sediments from the Tarfaya Basin (Morocco) comprise a well-studied Cenomanian–Turonian boundary interval (e.g. Tsikos et al., 2004). The focus of this study is on core S57, which contains ~37 m of cyclically bedded organic-rich calcareous sediments of Cenomanian–Turonian age, well dated with nannofossils and planktonic foramnifera, with a very low abundance of detrital minerals (Kolonic et al., 2005; Kuhnt et al., 2005). During deposition, the basin was located in an open shelf setting at ~15°N and is thought to have been fed by the upwelling of nutrient-rich waters (Lüning et al., 2004; Kolonic et al., 2005; Figure 1). Organic biomarker, Fe-speciation, and trace-metal data from high-resolution studies on part of this core, including the Plenus Cold Event interval, have revealed dominantly euxinic conditions with short intervals of anoxic non-sulfidic conditions (Kolonic et al., 2005; Poulton et al., 2015; Goldberg et al., 2016). Conditions in the Tarfaya Basin during deposition of the rest of the core were likely at least as reducing as implied by the generally higher Mo enrichments for these other intervals (Kolonic et al., 2005; Goldberg et al., 2016; Dickson et al., 2016).

2.2. Analytical methods

Aliquots of powdered sample material taken from archived samples of drill core S57 were weighed into Teflon digestion vessels together with a ^{113}Cd-^{111}Cd or ^{67}Zn-^{64}Zn double spike. The sample powders were digested on a hotplate for 48 hours in inverse aqua regia (iAR, 3 parts HNO_3, 1 part HCl) to preferentially dissolve authigenic shale components. Cd and Zn were separated from major-element cations and interferences in a two-stage anion column chromatography procedure modified from previous studies

(Dickson et al., 2016; Sweere et al., 2018; Sweere et al., 2020).

Stable-isotope analyses were performed on a Nu Instruments Plasma I multi-collector ICP-MS at the University of Oxford. Data were processed offline using an exponential mass-bias correction, measured relative to NIST-3108 Cd and IRMM-3702 Zn solutions, and reported as $\delta^{114}Cd = [^{114/110}Cd_{sample}/^{114/110}Cd_{NIST}]-1)*1000$ and $\delta^{66}Zn = [^{66/64}Zn_{sample}/^{66/64}Zn_{IRMM\text{-}3702}]-1) \times 1000 + 0.28$. External reproducibility was estimated based on repeated analyses of the USGS SDO-1 shale reference material: $\delta^{114}Cd_{SDO\text{-}1} = 0.13 \pm 0.06$ ‰ (2 SD, n = 5), and $\delta^{66}Zn_{SDO\text{-}1} = 0.43 \pm 0.07$ ‰ (2 SD, n=9). Reported errors in Figure 2 are the 2 standard error propagated uncertainties based on the reproducibility of the bracketing standards and the internal error of sample analysis. Enrichment factors (EF) are calculated relative to average upper continental crust concentrations as $TM_{EF} = (TM/Al)_{sample}/ (TM/Al)_{crust}$ (Rudnick and Gao, 2003, $Cd/Al_{crust} = 0.011 \times 10^4$; $Zn/Al_{crust} = 8.22 \times 10^4$ g/g).

2.3 English Chalk, Eastbourne

For comparison of the Tarfaya data to other sedimentary archives, Cd/Ca data for time-equivalent sediments from an outcrop near Eastbourne, UK are also presented. This section consists of organic-lean epicontinental pelagic nannofossil-rich deposits of the English Chalk, which have previously been studied for their $\delta^{66}Zn$ and Zn/Ca compositions (Jenkyns et al., 2017; Sweere et al., 2018). The previously unpublished Cd/Ca data presented here are from the same set of carbonate phase measurements presented by Jenkyns et al. (2017). Briefly, carbonates were selectively dissolved from bulk rock using 0.5M acetic acid. After centrifugation to remove undissolved sedimentary components, the supernatant was diluted to 10 ppm Ca, and measured on a Thermo Scientific Element 2 magnetic-sector ICP-MS.

2.4. Chemostratigraphic Divisions

To assess the environmental controls on stratigraphic δ^{114}Cd and δ^{66}Zn variations, samples for the Tarfaya core were grouped into different chemostratigraphic divisions, based mainly on the carbon-isotope stratigraphy. The shading of these different divisions, as indicated in Figure 2, are used later to compare metal concentrations and isotope compositions for these different intervals.

3. Results

Both Cd and Zn are strongly enriched in the Tarfaya sediments relative to upper continental crust. Values for Cd_{EF} range from ~20–850, with an average of 238 (n = 36); whilst those for Zn_{EF} range from ~3.2–207 and average 40 (n = 35). Enrichments of Zn and Cd follow similar stratigraphic patterns (Figure 2).

The Cd- and Zn-isotope compositions for the S57 core show stratigraphic patterns coincident with changes in other geochemical parameters. δ^{114}Cd values range from ~-0.61 to 0.26‰ with an average of -0.07‰ (n = 36). The maximum δ^{114}Cd values found for Tarfaya sediments approach the modern deep-ocean value of ~0.3‰ (e.g. Conway and John, 2015). The lowest δ^{114}Cd observed are considerably lower than dissolved δ^{114}Cd values generally found for the modern ocean and closer to values found in CdS precipitation experiments (Guinoiseau et al., 2018). δ^{66}Zn values range from ~-0.09 to 0.85‰ with an average of 0.32‰ (n = 38). The lowest δ^{66}Zn values observed are lower than those of the bulk silicate Earth (~0.3‰, Chen et al., 2013) and of riverine inputs (~0.3‰) but not lower than some estimates for Zn inputs from continental margins (~-0.8 to -0.5‰) or hydrothermal vents (~-0.5 to 0.3‰) (Conway and

John, 2014; compilation in Vance et al., 2016). The maximum δ^{66}Zn values observed are higher than dissolved δ^{66}Zn values measured for the modern deep ocean of δ^{66}Zn =0.5‰, but lower than some ocean outputs, including carbonates, which have average δ^{66}Zn values of ~ 0.9 ‰ and Fe-Mn oxyhydroxide crusts with values of ~1.0‰ (e.g. Pichat et al., 2003; Little et al., 2014).

The average δ^{114}Cd and δ^{66}Zn values for background conditions are -0.10 ± 0.09 (n = 17) and 0.31 ± 0.12 and (1 SD, n = 18), respectively (Figure 2). The Plenus Cold Event interval contains the lowest enrichments of Cd and Zn. This chemostratigraphic division also hosts the lowest isotope values for both Cd and Zn with average δ^{114}Cd and δ^{66}Zn values of -0.24 ± 0.23 and 0.14 ± 0.18 ‰, respectively (1 SD, n = 9). However, low δ^{114}Cd and δ^{66}Zn values during the Plenus Cold Event show different stratigraphic patterns. The highest δ^{114}Cd and δ^{66}Zn values are found in the stratigraphic interval just post-dating the Plenus Cold Event. Average δ^{114}Cd and δ^{66}Zn values observed for the plateau-phase of the OAE 2 interval are 0.11 ± 0.09 (n = 10) and 0.45 ± 0.23 (1 SD, n = 11), respectively. Cd/Ca values for the Eastbourne chalk vary between 0.019 and 0.19 μmol/mol with the highest values found in the interval of the Plenus Cold Event.

4. Discussion

The two most prominent features of the Tarfaya record are (i) higher Cd- and Zn-isotope values during the plateau phase of OAE 2 and (ii) a decrease in Cd- and Zn-isotope values during the PCE. The following discussion focuses on several key mechanisms that might account for the observed variations.

4.1. Hydrographic setting of the Tarfaya Basin

The degree and nature of water exchange between the Tarfaya Basin and the open ocean (proto-North Atlantic) are of critical importance in understanding stratigraphic δ^{114}Cd and δ^{66}Zn patterns because these phenomena control the amount and isotopic composition of dissolved Cd and Zn coming into the basin. The hydrographic conditions of the Tarfaya Basin can be evaluated using a Cd/Mo *vs* Co × Mn cross-plot, because modern organic-rich sediments have distinct Cd/Mo and Co × Mn values for different hydrographic regimes (Sweere et al., 2016).

Cd/Mo ratios of organic-rich marine sediments are thought to reflect the relative importance of export production *versus* preservation of organic material, due to the high Cd uptake in organic cellular material (Little et al., 2015; Sweere et al., 2016). Co and Mn concentrations are generally very low in sediments from oxygen minimum zones below upwelling regions, in contrast to restricted basins like the Black Sea (Brumsack, 2006; Sweere et al., 2016). These different geochemical signatures are thought to reflect the hydrographic conditions that impact both the supply and removal efficiencies of Co and Mn to the sediment.

Low removal efficiencies of Mn are expected in both restricted basins and upwelling settings, considering the high solubility of this element in reducing conditions (e.g. Tribovillard et al., 2006 and references therein). However, the supply of Mn and Co is likely to be higher in restricted basins as Co and Mn concentrations in rivers (and surface waters) are much higher than in open-ocean sub-surface waters that feed upwelling regions. With limited water exchange due to hydrographic restriction, these elements are effectively trapped in restricted basins, allowing higher dissolved and sedimentary concentrations to develop. Low supply in upwelling systems coupled to low removal efficiencies from seawater to sediment in OMZs allows these elements to be transported away from the OMZ and hence result in low sedimentary concentrations compared with those in restricted basins (Sweere et al., 2016).

An empirical comparison between elemental data from Tarfaya with modern marine sediment data suggests an open-ocean depositional regime for the Tarfaya Basin (Figure 3). This regime probably had relatively high primary productivity that was fed by upwelling of sub-surface waters from the proto-North Atlantic Ocean. Importantly, no significant difference in Cd/Mo *versus* Mn × Co relationships is observed between the three chemostratigraphic divisions, suggesting that the hydrographic conditions of the Tarfaya Basin remained relatively constant during the studied interval. This reconstruction agrees with previous suggestions that the Tarfaya Basin was situated in a region of active upwelling of nutrient-rich sub-surface waters from the proto-North Atlantic Ocean, promoting high primary productivity and high mass accumulation rates of organic carbon (Lüning et al., 2004; Kolonic et al., 2005; Trabucho-Alexandre et al., 2010; Dickson et al., 2016; Scholz et al., 2019).

4.2. Redox variations in the Tarfaya Basin

Despite the strong and relatively constant connection to the open ocean, there may have been variations in local redox conditions of the Tarfaya Basin that impacted Cd and Zn burial pathways and the isotopic offset between sediments and seawater. Temporarily more oxygenated conditions could have resulted in a larger isotopic offset between sediments and seawater, as found in modern continental-margin sediments (Little et al., 2016; Bryan, 2019). Such conditions would be comparable to sediments deposited in suboxic to anoxic environments in the modern ocean that show lower δ^{66}Zn values than sediments from the anoxic to mildly sulfidic Peru Margin (Little et al., 2016).

Mo_{EF} values provide an independent proxy for local redox conditions (Figures 2, 4, and 5; e.g. Scott and Lyons, 2012). Mo_{EF} values are generally high and reasonably constant for the S57 core, implying that anoxic to euxinic environments dominated conditions in the Tarfaya Basin during most of the studied interval (Kolonic et al., 2005; Dickson et al., 2016; Figures 2 and 4). While global drawdown of Mo may have occurred during the OAE 2 interval, there are no signs for severe local drawdown in the Tarfaya Basin; thus, stratigraphic patterns in Mo_{EF} are thought to mostly reflect local redox conditions (Dickson et al., 2016). Low Mo_{EF} values (<50) are almost exclusively limited to the Plenus Cold Event interval (Division 2), suggesting temporarily more oxygenated conditions. This interpretation of redox conditions in the Tarfaya Basin is generally consistent with a study on a different core (SN4), which concluded that conditions for the time-equivalent interval studied here were anoxic to mildly euxinic and relatively constant, apart from more oxygenated conditions during the Plenus Cold Event interval (Scholz et al., 2019).

The Plenus Cold Event interval also features the lowest δ^{114}Cd and δ^{66}Zn values for the S57 core, which could thus be the result of temporarily more oxidizing conditions. Stratigraphic patterns for both elements in sediments recording the Plenus Cold Event interval, however, are considerably different. δ^{114}Cd shows two abrupt perturbations to very low δ^{114}Cd (< -0.4‰), whereas δ^{66}Zn values display a gradual decrease throughout the interval. High-resolution TOC, Fe-speciation, and Mo data from previous studies on the same core offer a more detailed look at the possible impact of changing redox environments on δ^{114}Cd and δ^{66}Zn patterns during the Plenus Cold Event (Figure 5; Poulton et al., 2015; Dickson et al., 2016; Goldberg et al., 2016). The Fe-speciation data indicate euxinic conditions with brief, cyclically occurring shifts to anoxic non-sulfidic conditions. Patterns in Mo_{EF} do not vary systematically with the cyclic alternation in

Fe_{py}/Fe_{HR} and more closely resemble TOC patterns over this interval that show lower values for two intervals around 51 and 53 m depth (Figure 5).

Cross-plots of $\delta^{114}Cd$ and $\delta^{66}Zn$ with Mo_{EF} for all samples (Figure 4) can be considered alongside detailed stratigraphic information for the Plenus Cold Event interval (Figure 5) to assess the impact of local redox conditions on $\delta^{114}Cd$ and $\delta^{66}Zn$.

4.2.1 Local redox controls on $\delta^{114}Cd$

High $\delta^{114}Cd$ values for the carbon-isotope plateau phase (Figure 2) of the OAE interval can mostly be attributed to a change in $\delta^{114}Cd_{seawater}$ towards higher values, but some effect of changing local redox conditions cannot be excluded. There is a generally positive relationship observed between $\delta^{114}Cd$ and $Mo_{EF,}$ based on all samples (Figure 4), which implies there was a local redox control on the Cd-isotope composition of sediments in the Tarfaya Basin (Sweere et al., 2020). However, this positive relationship is absent within the different chemostratigraphic divisions separately, despite considerable variation in $\delta^{114}Cd$ and Mo_{EF} within them. Additionally, samples from the carbon-isotope plateau phase of the OAE 2 interval show consistently higher $\delta^{114}Cd$ values than background conditions, even for low Mo_{EF} samples, implying that there was likely a difference in $\delta^{114}Cd_{seawater}$ during deposition of sediments belonging to these two divisions.

Outliers with very low $\delta^{114}Cd$ values (< -0.4 ‰), deposited during the Plenus Cold Event interval (Division 2 in Figure 2), do suggest a larger isotopic offset between sediments and seawater as they all feature relatively low Mo_{EF} values. In a more detailed view of this interval (Figure 5), the lowest Cd-isotope values are not systematically registered in non-sulfidic intervals, only one of the two perturbations to low $\delta^{114}Cd$ being coincident with an interval of lower Fe_{py}/Fe_{HR} (Poulton et al., 2015; Figure 5). $\delta^{114}Cd$

patterns more closely follow trends in TOC and Mo_{EF}, with the lowest δ^{114}Cd consistently occurring in low-Mo_{EF} and -TOC intervals. The anomalously low δ^{114}Cd values (< -0.4‰) observed during the Plenus Cold Event are therefore attributed to a temporarily larger isotopic offset between seawater and sediments preserved under more oxygenated conditions.

When these samples (marked in red) are ignored, δ^{114}Cd values for the Plenus Cold Event interval (-0.09 ± 0.16 ‰, 2 S.D., n = 5) are comparable to those of the Cenomanian–Turonian background conditions (-0.10 ± 0.18 ‰) and lower than δ^{114}Cd values for the plateau phase of the carbon-isotope excursion (by up to ~0.3 ‰). δ^{114}Cd values for the remaining samples gradually drop to a minimum of ~-0.2‰ near the end of the Plenus Cold Event interval. This geochemical change cannot directly be explained by varying local redox conditions, as it changes independently of Mo_{EF} and Fe_{py}/Fe_{HR} patterns (Figure 5). More likely, this gradual stratigraphic change in δ^{114}Cd during the Plenus Cold Event reflects the evolution of $\delta^{114}Cd_{seawater}$ to lower values. This inferred perturbation to the global Cd-isotope cycle is consistent with elevated Cd/Ca ratios for the time-equivalent interval in the Eastbourne chalk, which indicates a substantial increase in dissolved Cd in seawater during the Plenus Cold Event (Figure 7).

4.2.2 Local redox controls on δ^{66}Zn

A cross-plot of δ^{66}Zn with Mo_{EF} values does not show a clear positive relationship, which implies local redox conditions were not the dominant control on δ^{66}Zn values of the Tarfaya Basin sediments. Samples with the lowest δ^{66}Zn values (0.0–0.1‰), found exclusively for the Plenus Cold Event interval, generally do show low Mo_{EF} values. However, there is no systematic relationship of stratigraphic δ^{66}Zn patterns with Fe_{py}/Fe_{HR}, Mo_{EF}, or TOC, for this interval (Figure 5) and therefore no apparent local redox or export productivity control on the decrease in δ^{66}Zn. The stratigraphic change in δ^{66}Zn values over the Plenus Cold Event interval is gradual, in contrast to patterns in Mo_{EF} and Fe_{py}/Fe_{HR} values that vary over shorter intervals. These observations imply that the transition to lower δ^{66}Zn values can largely be attributed to a change in the global seawater isotopic composition. Temporarily changing $\Delta^{66}Zn_{sediment-seawater}$, as a function of local redox conditions, would have likely led to more abrupt changes in sedimentary δ^{66}Zn values. This interpretation is consistent with a time-equivalent δ^{66}Zn shift of similar magnitude that has been found for organic-lean carbonate sediments from the Plenus Cold Event interval in southern England (Eastbourne) and southern Italy (Raia del Pedale) and was associated with higher Zn/Ca values (Figure 7, Sweere et al., 2018). Together, these studies provide strong evidence for a global perturbation to the Zn cycle during the Plenus Cold Event.

4.3 Concentrations of dissolved Cd and Zn

Sedimentary Cd and Zn concentrations relative to total organic carbon (TOC) can provide information on the availability of the dissolved elements. Low dissolved Mo concentrations in modern restricted euxinic basins have been shown to lead to proportionally lower Mo/TOC ratios in accumulating sediments (Algeo and Lyons, 2006) and a similar effect can be caused by the widespread removal of Mo from seawater during global anoxic episodes such as OAE 2 (van Bentum et al., 2009; Hetzel et al., 2009; Dickson et al., 2016, 2017; Owens et al., 2016). Considering the strong open-ocean connection (section 4.1), local drawdown of the dissolved Cd and Zn pool is unlikely to have impacted sedimentary enrichments for sediments of the Tarfaya Basin. Notably, Mo isotopes also do not display any evidence of periodic trace-metal drawdown at the study site (Dickson et al., 2016). More broadly, however, trace-metal drawdown in the wider proto-North Atlantic/Tethys region, or globally, could have impacted supply to the Tarfaya Basin and therefore the sedimentary Cd/TOC and Zn/TOC values.

Low Cd/TOC and, to a lesser extent, Zn/TOC values are observed for sediments from the intervals of the Plenus Cold Event (Division 2) and plateau-phase of the OAE 2 (Division 3), in comparison to background values (Division 1) (Figures 2, 6). For the Plenus Cold Event interval, these geochemical signatures can partly be explained by more oxygenated conditions, as indicated by low Mo_{EF} values, that would have limited the formation of sulfides. By contrast, samples from the plateau phase of the OAE 2 interval generally show high Mo_{EF} values, indicative of locally euxinic conditions, which would have enhanced export and burial of Cd and Zn relative to TOC as sulfides. Low Cd/TOC and Zn/TOC values for some of these samples therefore likely reflect the drawdown of the dissolved elements in the wider proto-North Atlantic/Tethys region or globally. This interpretation is consistent with anomalously low Zn concentrations that have been reported previously for the OAE 2 interval on the Demerara Rise (Hetzel et al., 2009; Owens et al., 2016).

4.4 The Cd- and Zn-isotope composition of Cenomanian–Turonian seawater

With relatively constant hydrographic (section 4.1) and redox (section 4.2) conditions in the Tarfaya Basin for the studied interval, the main influence on stratigraphic δ^{114}Cd and δ^{66}Zn patterns would have been the isotopic composition of the sub-surface proto-North Atlantic waters that fed the basin. The Cd- and Zn-isotope composition of the modern deep ocean is homogenous and set by the proportion of different inputs and outputs (e.g. Conway and John 2014; 2015, Vance et al., 2016; Weber et al., 2018). Reconstructions of sub-surface proto-North Atlantic δ^{114}Cd and δ^{66}Zn compositions may thus be used to infer changes in the global mass balance associated with paleoenvironmental change during the Cenomanian–Turonian interval. However, this interpretation requires some assumptions on $\Delta^{66}Zn_{sediment\text{-}seawater}$ and $\Delta^{114}Cd_{sediment\text{-}seawater}$ to be made.

4.4.1 Constraining $\delta^{114}Cd_{seawater}$ values

The limited amount of available modern data suggest a $\Delta^{114}Cd_{sediment\text{-}seawater}$ value of ~-0.3‰, for most organic-rich continental-margin sediments (Bryan, 2019). Application of this offset to the data presented here, excluding outliers in the Plenus Cold Event Interval (section 4.2), would imply a total range of Late Cretaceous $\delta^{114}Cd_{seawater}$ of 0.09 to 0.56 ‰. On average, $\delta^{114}Cd_{seawater}$ values for Division 1 (background conditions, 0.20 ± 0.09, 1 SD) and Division 2 (Plenus Cold Event, 0.21 ± 0.08 ‰, 1SD) are indistinguishable, and lower than values for Division 3 of Figure 2 (plateau phase, 0.41 ± 0.09 ‰, 1 SD). These values for Late Cretaceous $\delta^{114}Cd_{seawater}$ are plausible and roughly vary around the modern deep-ocean composition (~0.3 ‰). However, the uncertainties associated with these first reconstructions of Cenomanian–Turonian $\delta^{114}Cd_{seawater}$ values, further complicated by poor constraints on some aspects of the modern global isotopic mass balance, currently do not allow a meaningful quantitative assessment of variations in the global mass Cd mass balance during Late Cretaceous time.

4.4.2 Constraining $\delta^{66}Zn_{seawater}$ values

Of the three modern continental-margin sites for which $\delta^{66}Zn$ data are available (Peru Margin, Mexican Margin, California Borderland basins, Little et al., 2016), the highly reducing, highly productive conditions in the Tarfaya Basin were probably most comparable to the modern Peru Margin. This margin is characterized by high export productivity and organic-carbon burial rates, anoxic to mildly sulfidic (euxinic) conditions, and sediments with high TOC and total sulfur contents (Reimers and Suess, 1983; Suits and Arthur, 2000; Little et al., 2016). The studied Peru Margin sediments also feature a similar water depth (264 m) to that suggested for the Tarfaya Basin during Cenomanian–Turonian times (~200–300 m). δ^{66}Zn values of the Tarfaya Basin sediments may therefore be assumed to have been ~0.2‰ lower than the deep-ocean composition during the Late Cretaceous, similar to the difference for the present-day Peruvian Margin.

Applying a $\Delta^{66}\mathrm{Zn}_{\mathrm{sediment\text{-}seawater}}$ of -0.2‰ to all samples results in an average $\delta^{66}\mathrm{Zn}_{\mathrm{seawater}}$ composition for the proto-North Atlantic deep ocean during background conditions (Division 1 in Figure 2) of 0.51‰, which is indistinguishable from modern deep-ocean compositions (e.g. Conway and John, 2014). Based on a 3-point moving average, $\delta^{66}\mathrm{Zn}_{\mathrm{seawater}}$ values for the studied interval range from 0.14 to 0.76 ‰. The magnitude and timing of major stratigraphic trends are generally consistent with data from the Chalk of southern England at Eastbourne (Figure 7, Sweere et al., 2018). These observations thus support the inference of a change to the global zinc cycle, represented by its seawater composition, across an interval of widespread environmental change.

4.5 Drivers of $\delta^{66}\mathrm{Zn}_{\mathrm{seawater}}$ change

4.5.1 Defining the isotopic mass balance

A simplified global isotopic mass-balance model is used to assess the drivers of the reconstructed $\delta^{66}\mathrm{Zn}_{\mathrm{seawater}}$ change. In steady state, the total input flux (F_{input}) is equal to the sum of the outputs (F_{output}) into oxic (F_{ox}), anoxic (F_{anox}) and euxinic (F_{eux}) sediments so that $1 = f_{\mathrm{ox}} + f_{\mathrm{anox}} + f_{\mathrm{eux}}$. Here, f_{oxic} reflects Zn burial in Fe-Mn phases in oxic conditions (e.g. Little et al., 2014), f_{anoxic} refers to the Zn burial in organic-rich sediments on continental margins (Little et al., 2016), and $f_{euxinic}$ reflects the burial of Zn in strongly euxinic (restricted) basins, like the modern Black Sea (Vance et al., 2016; Isson et al., 2018).

The isotopic mass balance is as follows:

$$\delta^{66}Zn_{input} = \delta^{66}Zn_{oxic}*f_{oxic} + \delta^{66}Zn_{anoxic}*f_{anoxic} + \delta^{66}Zn_{euxinic}*f_{euxinic} \text{ (1),}$$

The isotopic composition of ocean outputs can all be expressed relative to the seawater isotope composition ($\Delta^{66}Zn_{output\text{-}sw} = \delta^{66}Zn_{output} - \delta^{66}Zn_{seawater}$). By combining the two equations above, the Zn-isotope composition of seawater can then be expressed as a function of f_{anox} and f_{eux} as:

$$\delta^{66}Zn_{sw} = (\Delta^{66}Zn_{oxic\text{-}sw} - \Delta^{66}Zn_{anox\text{-}sw})*f_{anox} + (\Delta^{66}Zn_{oxic\text{-}sw} - \Delta^{66}Zn_{eux\text{-}sw})*f_{eux} + \delta^{66}Zn_{input} - \Delta^{66}Zn_{oxic\text{-}sw} \text{ (2).}$$

By assuming f_{eux} is a fixed proportion (b) of f_{anox} (i.e. $f_{eux} = b \times f_{anox}$), $\delta^{66}Zn_{sw}$ can then be plotted against f_{anox} (Figure 8). Here, the gradient is given by $(\Delta^{66}Zn_{oxic\text{-}sw} - \Delta^{66}Zn_{anox\text{-}sw}) + (\Delta^{66}Zn_{oxic\text{-}sw} - \Delta^{66}Zn_{eux\text{-}sw}) \times b$, and the *y*-axis intercept by $\delta^{66}Zn_{input} - \Delta^{66}Zn_{oxic\text{-}sw}$.

4.5.1 The Plenus Cold Event interval and pre-OAE $\delta^{66}Zn$ excursion.

This isotopic mass-balance model implies that the inferred drop in the $\delta^{66}Zn_{seawater}$ value for the Plenus Cold Event interval reflects a global decrease in the proportion of Zn removal into anoxic organic-rich sediments relative to oxic sediments (Figure 8). This interpretation is consistent with U-isotope evidence for a more oxygenated seafloor during the Plenus Cold Event (Clarkson et al., 2018). These lower $\delta^{66}Zn_{seawater}$ values also might reflect the remobilization of previously buried isotopically light Zn from organic-rich continental-margin sediments following large-scale ocean oxygenation (cf. Conway and John, 2014; Lemaitre et al., 2020), alongside other chalcophilic and redox-sensitive trace metals as inferred for data from carbonate successions for this interval (Jenkyns et al., 2017; Clarkson et al., 2018; Sweere et al., 2018). Spikes in concentrations of the trace metals Co, Cu, Sc, and Cr, and the negative shift in Cr isotopes, as found in sediments from the Western Interior Seaway, have also been linked to mafic input from the Caribbean and High Arctic Large Igneous Provinces (LIPs) during the Plenus Cold Event interval (e.g. Eldrett et al., 2014; Holmden et al., 2016). This mafic event may have also impacted the Zn (and Cd) cycle and contributed to an inferred lower $\delta^{66}Zn_{seawater}$ value for this interval.

Another negative shift in $\delta^{66}Zn$ values of similar magnitude has been observed in European carbonate archives stratigraphically just below the onset of the carbon-isotope excursion that defines the OAE 2 interval (Sweere et al., 2018). This drop in $\delta^{66}Zn$ values could represent a particularly strong pulse of isotopically light Zn to the ocean from hydrothermal fluids or low-temperature reactions between seawater and mafic rocks due to the onset of a LIP, for which there is independent evidence from the global osmium-isotope record (Turgeon and Creaser, 2008; Du Vivier et al., 2014, 2015). The corresponding interval in the Tarfaya succession also features anomalously low $\delta^{66}Zn$ values, as well as low $\delta^{114}Cd$ values (Figure 7). These observations provide support for a direct link between the onset of a major magmatic episode and ocean nutrification as a trigger for increased carbon burial.

4.5.2 Carbon-isotopic plateau-phase of the OAE 2 interval

Higher $\delta^{66}Zn_{seawater}$ values for the plateau phase of the OAE 2 interval require a higher proportion of isotopically light Zn burial into anoxic organic-rich sediments relative to background conditions (Figure 8). An increase of ~0.25‰ for the plateau phase of the OAE interval, from 0.5 to 0.75‰, would have required most of the Zn output to have been into anoxic organic-rich sediments. This interpretation is generally consistent with evidence from other proxies. Mn-oxide burial is estimated to have decreased by 40 to 80% associated with a positive thallium-isotope shift during the OAE 2 interval (Ostrander et al., 2017), so a decrease in Zn burial in oxic sediments of similar magnitude is likely. Organic-carbon burial rates during OAE 2 are estimated to be ~1.7 to 3.1 times higher than modern ocean burial rates based on TOC and $\delta^{13}C$ patterns (Owens et al., 2018).

The current uncertainties in the quantitative interpretation of the global Zn-isotope mass balance changes may be improved by: (i) The analysis of OAE 2 sediments from other sites, to constrain $\delta^{66}Zn_{seawater}$ more accurately; (ii) Improved understanding of the processes leading to isotopic differences between seawater and various sediment types in the modern ocean, particularly for organic-rich continental- margin sediments; and (iii) Better constraints on possible past variations in $\delta^{66}Zn_{input}$, through assessment of the flux and isotopic composition of Zn inputs from hydrothermal systems, LIPs, and sedimentary sources.

4.6 Comparing $\delta^{114}Cd$ and $\delta^{66}Zn$

Despite uncertainties on the absolute values of the Cd-isotope composition of the Cenomanian–Turonian ocean, the relative changes are clear and generally show a remarkably similar stratigraphic pattern to $\delta^{66}Zn$. A strong correlation in a cross-plot of

Cd and Zn concentrations implies that local controls on export and burial of these elements were also generally similar. However, δ^{114}Cd *versus* δ^{66}Zn reveals considerable scatter (Figure 9). Most notably, δ^{114}Cd values comprise a much smaller range and values for the Plenus Cold Event interval are similar to background values for the OAE 2 interval, while δ^{66}Zn values show considerably lower values. This contrast may reflect the lack of a Cd output flux heavier than seawater compositions, in contrast to Zn where oxic outputs provide a substantial sink of isotopically heavy Zn (e.g. Little et al., 2014). Additionally, the disparity in δ^{114}Cd *versus* δ^{66}Zn values may reflect differences in the isotopic composition of ocean inputs. Zn may be more easily remobilized from continental-margin sediments or have a larger, more isotopically distinct hydrothermal/volcanic source signatures (Lemaitre et al., 2020), as also implied by comparison of dissolved δ^{114}Cd and δ^{66}Zn patterns from the North Atlantic Ocean (Conway and John, 2014; 2015). A substantial input of isotopically light Zn from enhanced basalt-seawater interaction or the release from continental-margin sediments associated with large-scale oxygenation during the Plenus Cold Event may explain differences in δ^{66}Zn and δ^{114}Cd patterns.

5. Conclusions

- Stratigraphic patterns of δ^{114}Cd and δ^{66}Zn in the Tarfaya Basin S57 core (Morocco) can largely be interpreted as a result of changing seawater values. The location of the Tarfaya Basin in an upwelling zone on the margins of the proto North-Atlantic Ocean suggests that the δ^{114}Cd and δ^{66}Zn values of seawater supplied to the basin represent sub-surface conditions and may thus be extrapolated to infer changes in the global mass balance of these elements.

- A combination of Cd and Zn concentrations relative to TOC, Mo enrichments, and δ^{114}Cd and δ^{66}Zn values of the sediments suggests ocean-wide drawdown of Cd and Zn resulting from extensive organic-rich sediment burial during the main phase of the OAE. This drawdown is expressed as isotopic shifts of ~ +0.2–0.3 ‰ in the δ^{114}Cd and δ^{66}Zn composition of sub-surface waters, relative to background conditions.
- Pelagic carbonate (English Chalk, Eastbourne) and organic-rich sedimentary archives (Tarfaya) from different oceanic regimes record similar stratigraphic patterns in δ^{66}Zn during the Cenomanian–Turonian interval, particularly during the Plenus Cold Event. The similarities imply that common changes in the δ^{66}Zn stratigraphy derive from the oceanic dissolved δ^{66}Zn, and that these archives record global palaeo-environmental information.
- Perturbations to the global Zn cycle during the Plenus Cold Event are suggested to reflect widespread ocean re-oxygenation, thereby lowering the fraction of isotopically light Zn buried in organic-rich sediments and possibly re-mobilizing previously buried isotopically light material by the oxygenation of organic-rich sediments. The increased input of isotopically light Zn from enhanced basalt-seawater interaction during this interval may have also contributed to relatively low δ^{66}Zn values.

Acknowledgements

We thank Alan Hsieh and Philip Holdship for laboratory support, Sander van den Boorn for his contribution in an early phase of the project, and Shell Global Solutions International B.V. for research funding. We gratefully acknowledge constructive reviews by Seth John and one anonymous reviewer that helped to improve our manuscript.

References

Algeo, T.J., Lyons, T.W., 2006. Mo–total organic carbon covariation in modern anoxic marine environments: Implications for analysis of paleoredox and paleohydrographic conditions. *Paleoceanography* 21, PA1016, https://doi.org/10.1029/2004PA001112.

Arthur, M.A., Jenkyns, H.C., Brumsack, H.-J., Schlanger S.O., 1990. Stratigraphy, geochemistry, and paleoceanography of organic-carbon-rich Cretaceous sequences, in *Cretaceous Resources, Events and Rhythms,* edited by R.N. Ginsburg and B. Beaudoin, NATO ASI Series, Kluwer Academic Publishers, Dordrecht, 304, 75–119.

Bruland, K.W., 1980. Oceanographic distributions of cadmium, zinc, nickel, and copper in the North Pacific. *Earth and Planetary Science Letters* 47, 176–198, https://doi.org/10.1016/0012-821x(80)90035-7.

Brumsack, H.-J., 2006. The trace metal content of recent organic carbon-rich sediments: implications for Cretaceous black shale formation. *Palaeogeography, Palaeoclimatology, Palaeoecology 232*, 344–361, https://doi.org/10.1016/j.palaeo.2005.05.011.

Bryan, A., 2019. Investigation of the controls on the cadmium isotope composition of modern marine sediments. DPhil thesis, University of Oxford.

Chen, H., Savage, P.S., Teng, F.-Z., Helz, R.T., Moynier, F., 2013. Zinc isotope fractionation during magmatic differentiation and the isotopic composition of the bulk Earth. *Earth and Planetary Science Letters* 369, 34–42, https://doi.org/10.1016/j.epsl.2013.02.037.

Clarkson, M. O., Stirling, C. H., Jenkyns, H. C., Dickson, A. J., Porcelli, D., Moy, C. M., Pogge von Strandmann, P. A. E., Cooke, I. R., Lenton, T. M., 2018. Uranium isotope evidence for two episodes of deoxygenation during Oceanic Anoxic Event 2. *Proceedings of the National Academy of Sciences*, 115(12), 2918–2923.

Conway, T.M., John, S.G., 2014. The biogeochemical cycling of zinc and zinc isotopes in the North Atlantic Ocean. *Global Biogeochemical Cycles* 28, 1111–1128, https://doi.org/10.1002/2014GB004862.

Conway, T.M., John, S.G., 2015. Biogeochemical cycling of cadmium isotopes along a high-resolution section through the North Atlantic Ocean. *Geochimica et Cosmochimica Acta* 148, 269–283, https://doi.org/10.1016/j.gca.2014.09.032.

De Souza, G. F., Khatiwala, S. P., Hain, M. P., Little, S. H., & Vance, D., 2018. On the origin of the marine zinc–silicon correlation. Earth and Planetary Science Letters, 492, 22–34.

Dong, S., & Wasylenki, L. E., 2016. Zinc isotope fractionation during adsorption to calcite at high and low ionic strength. *Chemical Geology*, 447, 70–78, https://doi.org/10.1016/j.chemgeo.2016.10.031.

Dickson, A., 2017. A molybdenum isotope perspective on Phanerozoic deoxygenation events. *Nature Geoscience* 10, 721–726, https://doi:10.1038/ngeo527.

Dickson, A.J., Jenkyns, H.C., Porcelli, D., van den Boorn, S., Idiz, E., 2016. Basin-scale controls on the molybdenum-isotope composition of seawater during Oceanic Anoxic Event 2 (Late Cretaceous). *Geochimica et Cosmochimica Acta* 178, 291–306, https://doi.org/10.1016/j.gca.2015.12.036.

Dickson, A.J., Saker- Clark, M., Jenkyns, H.C., Bottini, C., Erba, E., Russo, F., Gorbanenko, O., Naafs, B.D., Pancost, R.D., Robinson, S.A., 2017. A Southern Hemisphere record of global trace- metal drawdown and orbital modulation of organic- matter burial across the Cenomanian–Turonian boundary (Ocean Drilling Program Site 1138, Kerguelen Plateau). *Sedimentology* 64, 186–203, https://doi.org/10.1111/sed.12303.

Du Vivier, A. D., Selby, D., Sageman, B. B., Jarvis, I., Gröcke, D. R., & Voigt, S., 2014. Marine ^{187}Os/^{188}Os isotope stratigraphy reveals the interaction of volcanism and ocean circulation during Oceanic Anoxic Event 2. *Earth and Planetary Science Letters*, 389, 23–33, https://doi.org/10.1016/j.epsl.2013.12.024.

Du Vivier, A. D. C., Selby, D., Condon, D. J., Takashima, R., & Nishi, H., 2015. Pacific $^{187}Os/^{188}Os$ isotope chemistry and U–Pb geochronology: Synchroneity of global Os isotope change across OAE 2. *Earth and Planetary Science Letters*, 428, 204–216, https://doi.org/10.1016/j.epsl.2015.07.020.

Eldrett, J.S., Minisini, D., Bergman, S.C., 2014. Decoupling of the carbon cycle during Ocean Anoxic Event 2. *Geology* 42, 567–570, https://doi.org/10.1130/G35520.1.

Forster, A., Schouten, S., Moriya, K., Wilson, P. A., & Sinninghe Damsté, J. S., 2007. Tropical warming and intermittent cooling during the Cenomanian/Turonian oceanic anoxic event 2: Sea surface temperature records from the equatorial Atlantic. *Paleoceanography*, 22(1).

Gale, A.S., Christensen, W.K., Gale, A., 1996. Occurrence of the belemnite *Actinocamax plenus* in the Cenomanian of SE France and its significance, *Bulletin of the Geological Society of Denmark* 43, 68–77.

Gale, A.S., Jenkyns, H.C., Tsikos, H., van Breugel, Y., Sinninghe Damste, J.S., Bottini, C., Erba, E., Russo, F., Falzoni, F., Petrizzo, M.R., Dickson, A.J., 2019. High--resolution bio-and chemostratigraphy of an expanded record of Oceanic Anoxic Event 2 (Late Cenomanian–Early Turonian) at Clot Chevalier, near Barrême, SE France (Vocontian Basin, SE France). *Newsletters on Stratigraphy* 52, 97–129, https://doi.org/ 10.1127/nos/2018/0445.

Gangl, S.K., Moy, C.M., Stirling, C.H., Jenkyns, H.C., Crampton, J.S., Clarkson, M.O., Ohneiser, C., Porcelli, D., 2019. High-resolution records of Oceanic Anoxic Event 2: Insights into the timing, duration and extent of environmental perturbations from the palaeo-South Pacific Ocean. *Earth and Planetary Science Letters* 518, 172–182, https://doi.org/10.1016/j.epsl.2019.04.028.

Goldberg, T., Poulton, S.W., Wagner, T., Kolonic, S.F., Rehkämper, M., 2016. Molybdenum drawdown during Cretaceous oceanic anoxic event 2. *Earth and Planetary Science Letters* 440, 81–91, https://doi.org/10.1016/j.epsl.2016.02.006.

Guinoiseau, D., Galer, S.J., Abouchami, W., 2018. Effect of cadmium sulfide precipitation on the partitioning of Cd isotopes: Implications for the oceanic Cd cycle. *Earth and Planetary Science Letters* 498, 300–308, https://doi.org/10.1016/j.epsl.2018.06.039.

Hetzel, A., Böttcher, M.E., Wortmann, U.G., Brumsack, H.-J., 2009. Paleo-redox conditions during OAE 2 reflected in Demerara Rise sediment geochemistry (ODP Leg 207). *Palaeogeography, Palaeoclimatology, Palaeoecology* 273, 302–328, https://doi.org/10.1016/j.palaeo.2008.11.005.

Holmden, C., Jacobson, A.D., Sageman, B.B., Hurtgen, M.T., 2016. Response of the Cr isotope proxy to Cretaceous Ocean Anoxic Event 2 in a pelagic carbonate succession from the Western Interior Seaway. *Geochimica et Cosmochimica Acta* 186, 277–295, https://doi.org/10.1016/j.gca.2016.04.039.

Horner, T., Schönbächler, M., Rehkämper, M., Nielsen, S., Williams, H., Halliday, A., Xue, Z., Hein, J., 2010. Ferromanganese crusts as archives of deep water Cd isotope compositions. *Geochemistry, Geophysics, Geosystems* 11, Q04001 https://doi.org/10.1029/2009GC002987.

Isson, T.T., Love, G.D., Dupont, C.L., Reinhard, C.T., Zumberge, A.J., Asael, D., Gueguen, B., McCrow, J., Gill, B.C. and Owens, J., 2018. Tracking the rise of eukaryotes to ecological dominance with zinc isotopes. *Geobiology* 16, 341–352, https://doi.org/10.1111/gbi.12289.

Janssen, D. J., Abouchami, W., Galer, S. J., Purdon, K. B., & Cullen, J. T., 2019. Particulate cadmium stable isotopes in the subarctic northeast Pacific reveal dynamic Cd cycling and a new isotopically light Cd sink. *Earth and Planetary Science Letters*, 515, 67–78, https://doi.org/10.1016/j.epsl.2019.03.006.

Jarvis, I., Lignum, J.S., Gröcke, D.R., Jenkyns, H.C., Pearce, M.A., 2011. Black shale deposition, atmospheric CO_2 drawdown, and cooling during the Cenomanian–Turonian Oceanic Anoxic Event. *Paleoceanography* 26, PA3201, https://doi.org/10.1029/2010PA002081.

Jenkyns, H.C., 2010. Geochemistry of oceanic anoxic events. *Geochemistry, Geophysics, Geosystems* 11, Q03004, https://doi.org/10.1029/2009GC002788.

Jenkyns, H.C., Dickson, A.J., Ruhl, M., van den Boorn, S.H.J.M., 2017. Basalt–seawater interaction, the Plenus Cold Event, enhanced weathering and geochemical change:

deconstructing Oceanic Anoxic Event 2 (Cenomanian–Turonian, Late Cretaceous). *Sedimentology* 64, 16–43, https://doi.org/10.1111/sed.12305.

John, S. G., Geis, R. W., Saito, M. A., & Boyle, E. A., 2007. Zinc isotope fractionation during high-affinity and low-affinity zinc transport by the marine diatom Thalassiosira oceanica. Limnology and Oceanography, 52(6), 2710–2714.

John, S.G., Kunzmann, M., Townsend, E.J., Rosenberg, A.D., 2017. Zinc and cadmium stable isotopes in the geological record: A case study from the post-snowball Earth Nuccaleena cap dolostone. *Palaeogeography, Palaeoclimatology, Palaeoecology* 466, 202–208, https://doi.org/10.1016/j.palaeo.2016.11.003.

John, S.G., Rouxel, O.J., Craddock, P.R., Engwall, A.M., Boyle, E.A., 2008. Zinc stable isotopes in seafloor hydrothermal vent fluids and chimneys. *Earth and Planetary Science Letters* 269, 17–28, doi.org/10.1016/j.epsl.2007.12.011.

Köbberich, M., & Vance, D., 2019. Zn isotope fractionation during uptake into marine phytoplankton: Implications for oceanic zinc isotopes. *Chemical Geology*, 523, 154–161.

Kolonic, S., Wagner, T., Forster, A., Sinninghe Damsté, J.S., Walsworth- Bell, B., Erba, E., Turgeon, S., Brumsack, H.J., Chellai, E.H., Tsikos, H., 2005. Black shale deposition on the northwest African Shelf during the Cenomanian/Turonian oceanic anoxic event: Climate coupling and global organic carbon burial. *Paleoceanography* 20, PA1006 https://doi.org/10.1029/2003PA000950.

Kraal, P., Slomp, C. P., Forster, A., & Kuypers, M. M., 2010. Phosphorus cycling from the margin to abyssal depths in the proto-Atlantic during oceanic anoxic event 2. *Palaeogeography, Palaeoclimatology, Palaeoecology* 295(1-2), 42–54. https://doi.org/10.1016/j.palaeo.2010.05.014

Kuhnt, W., Luderer, F., Nederbragt, S., Thurow, J., Wagner, T., 2005. Orbital-scale record of the late Cenomanian–Turonian oceanic anoxic event (OAE-2) in the Tarfaya Basin (Morocco). *International Journal of Earth Sciences* 94, 147–159, https://doi.org/10.1007/s00531-004-0440-5.

Kuypers, M.M., van Breugel, Y., Schouten, S., Erba, E., Damsté, J.S.S., 2004. N_2-fixing cyanobacteria supplied nutrient N for Cretaceous oceanic anoxic events. *Geology* 32, 853–856, https://doi.org/10.1130/G20458.1.

Lemaitre, N., de Souza, G. F., Archer, C., Wang, R. M., Planquette, H., Sarthou, G., & Vance, D., 2020. Pervasive sources of isotopically light zinc in the North Atlantic Ocean. Earth and Planetary Science Letters, 539, 116216, https://doi.org/10.1016/j.epsl.2020.116216.

Little, S.H., Vance, D., Walker-Brown, C., Landing, W.M., 2014. The oceanic mass balance of copper and zinc isotopes, investigated by analysis of their inputs, and outputs to ferromanganese oxide sediments. *Geochimica et Cosmochimica Acta* 125, 673–693, https://doi.org/10.1016/j.gca.2013.07.046.

Little, S.H., Vance, D., Lyons, T.W., McManus, J., 2015. Controls on trace metal authigenic enrichment in reducing sediments: insights from modern oxygen-deficient settings. *American Journal of Science* 315, 77–119, https://doi.org/10.2475/02.2015.01.

Little, S.H., Vance, D., McManus, J., Severmann, S., 2016. Key role of continental margin sediments in the oceanic mass balance of Zn and Zn isotopes. *Geology* 44, 207–210, https://doi.org/10.1130/G37493.1.

Lüning, S., Kolonic, S., Belhadj, E., Belhadj, Z., Cota, L., Barić, G., Wagner, T., 2004. Integrated depositional model for the Cenomanian–Turonian organic-rich strata in North Africa. *Earth-Science Reviews* 64, 51–117, https://doi.org/10.1016/S0012-8252(03)00039-4.

Meyers, S.R., Sageman, B.B., Arthur, M.A., 2012. Obliquity forcing of organic matter accumulation during Oceanic Anoxic Event 2. *Paleoceanography* 27, PA3212. https://doi.org/10.1029/2012PA002286.

Monteiro, F., Pancost, R., Ridgwell, A., Donnadieu, Y., 2012. Nutrients as the dominant control on the spread of anoxia and euxinia across the Cenomanian-Turonian oceanic anoxic event (OAE2): Model–data comparison. *Paleoceanography* 27, PA4209 https://doi.org/10.1029/2012PA002351.

Morel, F. M. M., Reinfelder, J. R., Roberts, S. B., Chamberlain, C. P., Lee, J. G., & Yee, D., 1994. Zinc and carbon co-limitation of marine phytoplankton. *Nature* 369 (6483), 740.

Mort, H.P., Adatte, T., Föllmi, K.B., Keller, G., Steinmann, P., Matera, V., Berner, Z., Stüben, D., 2007. Phosphorus and the roles of productivity and nutrient recycling during oceanic anoxic event 2. *Geology* 35, 483–486, https://doi.org/10.1130/G23475A.1.

Muller- Karger, F.E., Varela, R., Thunell, R., Luerssen, R., Hu, C., Walsh, J.J., 2005. The importance of continental margins in the global carbon cycle. *Geophysical research letters* 32, https://doi.org/10.1029/2004GL021346.

O'Brien, C.L., Robinson, S.A., Pancost, R.D., Damsté, J.S.S., Schouten, S., Lunt, D.J., Alsenz, H., Bornemann, A., Bottini, C., Brassell, S.C., 2017. Cretaceous sea-surface temperature evolution: Constraints from TEX86 and planktonic foraminiferal oxygen isotopes. *Earth-science reviews* 172, 224–247, https://doi.org/10.1016/j.earscirev.2017.07.012.

O'Connor, L.K., Jenkyns, H.C., Robinson, S.A., Remmelzwaal, S.R., Batenburg, S.J., Parkinson, I.J. and Gale, A.S., 2020. A re- evaluation of the Plenus Cold Event, and the links between CO2, temperature, and seawater chemistry during OAE 2. *Paleoceanography and Paleoclimatology*, 35(4), e2019PA003631, https://doi.org/10.1029/2019PA003631.

Ostrander, C. M., Owens, J. D., & Nielsen, S. G., 2017. Constraining the rate of oceanic deoxygenation leading up to a Cretaceous Oceanic Anoxic Event (OAE-2:~ 94 Ma). *Science advances*, 3(8), e1701020, https://doi.org/10.1126/sciadv.1701020.

Owens, J.D., Reinhard, C.T., Rohrssen, M., Love, G.D., Lyons, T.W., 2016. Empirical links between trace metal cycling and marine microbial ecology during a large perturbation to Earth's carbon cycle. *Earth and Planetary Science Letters* 449, 407–417, https://doi.org/10.1016/j.epsl.2016.05.046.

Owens, J. D., Lyons, T. W., & Lowery, C. M., 2018. Quantifying the missing sink for global organic carbon burial during a Cretaceous oceanic anoxic event. *Earth and Planetary Science Letters*, 499, 83–94, https://doi.org/10.1016/j.epsl.2018.07.021.

Pichat, S., Douchet, C., Albarède, F., 2003. Zinc isotope variations in deep-sea carbonates from the eastern equatorial Pacific over the last 175 ka. *Earth and Planetary Science Letters* 210, 167–178, https://doi.org/10.1016/S0012-821X(03)00106-7.

Poulton, S.W., Henkel, S., März, C., Urquhart, H., Flögel, S., Kasten, S., Damsté, J.S.S., Wagner, T., 2015. A continental-weathering control on orbitally driven redox-nutrient cycling during Cretaceous Oceanic Anoxic Event 2. *Geology* 43, 963–966, https://doi.org/10.1130/G36837.1.

Reimers, C. E., & Suess, E., 1983. Spatial and temporal patterns of organic matter accumulation on the Peru continental margin. In Coastal Upwelling: Its Sediment Record, edited by J. Theide and E. Suess, 10, 163–180. Plenum, New York.

Roshan, S., Wu, J., 2015. Water mass mixing: The dominant control on the zinc distribution in the North Atlantic Ocean. *Global Biogeochemical Cycles* 29, 1060–1074, https://doi.org/10.1002/2014GB005026.

Roshan, S., Wu, J., Jenkins, W.J., 2016. Long-range transport of hydrothermal dissolved Zn in the tropical South Pacific. *Marine Chemistry* 183, 25–32, https://doi.org/10.1016/j.marchem.2016.05.005.

Rudnick, R.L., Gao, S., 2003. Composition of the continental crust. *Treatise on geochemistry* 3, 1–64, https://doi.org/10.1016/B0-08-043751-6/03016-4.

Schlanger, S.O., Jenkyns, H., 1976. Cretaceous oceanic anoxic events: causes and consequences. *Geologie en Mijnbouw* 55, 179–184.

Schmitt, A.-D., Galer, S.J., Abouchami, W., 2009. Mass-dependent cadmium isotopic variations in nature with emphasis on the marine environment. *Earth and Planetary Science Letters* 277, 262–272, https://doi.org/10.1016/j.epsl.2008.10.025.

Scholz, F., 2018. Identifying oxygen minimum zone-type biogeochemical cycling in Earth history using inorganic geochemical proxies. *Earth-Science Reviews*, https://doi.org/10.1016/j.earscirev.2018.08.002.

Scholz, F., Beil, S., Flögel, S., Lehmann, M. F., Holbourn, A., Wallmann, K., & Kuhnt, W., 2019. Oxygen minimum zone-type biogeochemical cycling in the Cenomanian-Turonian Proto-North Atlantic across Oceanic Anoxic Event 2. *Earth and Planetary Science Letters* 517, 50–60, https://doi.org/10.1016/j.epsl.2019.04.008.

Scholz, F., & Neumann, T., 2007. Trace element diagenesis in pyrite-rich sediments of the Achterwasser lagoon, SW Baltic Sea. Marine Chemistry, 107(4), 516-532, https://doi.org/10.1016/j.marchem.2007.08.005.

Scott, C., & Lyons, T. W., 2012. Contrasting molybdenum cycling and isotopic properties in euxinic versus non-euxinic sediments and sedimentary rocks: Refining the paleoproxies. *Chemical Geology*, 324, 19–27.

Sieber, M., Conway, T. M., de Souza, G. F., Hassler, C. S., Ellwood, M. J., & Vance, D., 2020. Cycling of zinc and its isotopes across multiple zones of the Southern Ocean: Insights from the Antarctic Circumnavigation Expedition. *Geochimica et Cosmochimica Acta*, 268, 310–324.

Sinninghe Damsté, J. S., van Bentum, E. C., Reichart, G. J., Pross, J., & Schouten, S. (2010). A CO_2 decrease-driven cooling and increased latitudinal temperature gradient during the mid-Cretaceous Oceanic Anoxic Event 2. *Earth and Planetary Science Letters*, 293(1-2), 97–103. https://doi.org/10.1016/j.epsl.2010.02.027.

Suits, N. S., & Arthur, M. A., 2000. Sulfur diagenesis and partitioning in Holocene Peru shelf and upper slope sediments. *Chemical Geology*, 163(1-4), 219–234.

Sweere, T., van den Boorn, S., Dickson, A.J., Reichart, G.-J., 2016. Definition of new trace-metal proxies for the controls on organic matter enrichment in marine sediments based on Mn, Co, Mo and Cd concentrations. *Chemical Geology* 441, 235–245, https://doi.org/10.1016/j.chemgeo.2016.08.028.

Sweere, T.C., Dickson, A.J., Jenkyns, H.C., Porcelli, D., Elrick, M., van den Boorn, S.H., Henderson, G.M., 2018. Isotopic evidence for changes in the zinc cycle during Oceanic Anoxic Event 2 (Late Cretaceous). *Geology* 46, 463–466, https://doi.org/10.1130/G40226.1.

Sweere, T. C., Dickson, A. J., Jenkyns, H. C., Porcelli, D., Ruhl, M., Murphy, M. J., Idiz, E., Van den Boorn, S.H.J.M., Eldrett, J.S., Henderson, G. M. 2020. Controls on the Cd-isotope composition of Upper Cretaceous (Cenomanian–Turonian) organic-rich mudrocks from south Texas (Eagle Ford Group). *Geochimica et Cosmochimica Acta*, https://doi.org/10.1016/j.gca.2020.02.019.

Trabucho Alexandre, J., Tuenter, E., Henstra, G.A., van der Zwan, K.J., van de Wal, R.S., Dijkstra, H.A., de Boer, P.L., 2010. The mid-Cretaceous North Atlantic nutrient trap: Black shales and OAEs. *Paleoceanography* 25, PA4201, https://doi.org/10.1029/2010PA001925.

Tsikos, H., Jenkyns, H., Walsworth-Bell, B., Petrizzo, M., Forster, A., Kolonic, S., Erba, E., Silva, I.P., Baas, M., Wagner, T., 2004. Carbon-isotope stratigraphy recorded by the Cenomanian–Turonian Oceanic Anoxic Event: correlation and implications based on three key localities. *Journal of the Geological Society* 161, 711–719, https://doi.org/10.1144/0016-764903-077.

Turgeon, S. C., & Creaser, R. A. (2008). Cretaceous oceanic anoxic event 2 triggered by a massive magmatic episode. *Nature* 454(7202), 323, https://doi.org/10.1038/nature07076.

van Bentum, E. C., Hetzel, A., Brumsack, H. J., Forster, A., Reichart, G. J., & Damste, J. S. S. (2009). Reconstruction of water column anoxia in the equatorial Atlantic during the Cenomanian–Turonian oceanic anoxic event using biomarker and trace metal proxies. *Palaeogeography, Palaeoclimatology, Palaeoecology*, 280(3-4), 489–498.

van Helmond, N. A., Ruvalcaba Baroni, I., Sluijs, A., Sinninghe Damsté, J. S., & Slomp, C. P., 2014. Spatial extent and degree of oxygen depletion in the deep proto-North Atlantic basin during Oceanic Anoxic Event 2. *Geochemistry, Geophysics, Geosystems*, 15(11), 4254–4266.

van Helmond, N. A.G.M., Sluijs, A., Papadomanolaki, N. M., Plint, A. G., Gröcke, D. R., Pearce, M. A., Eldrett, J. S., Trabucho-Alexandre, J., Walaszczyk, I., van de Schootbrugge, B., Brinkhuis, H. 2016. Equatorward phytoplankton migration during a cold spell within the Late Cretaceous super-greenhouse. *Biogeosciences*, 13(9), 2859–2872.

Vance, D., Little, S.H., Archer, C., Cameron, V., Andersen, M.B., Rijkenberg, M.J., Lyons, T.W., 2016. The oceanic budgets of nickel and zinc isotopes: the importance of sulfidic environments as illustrated by the Black Sea. Phil. Trans. R. Soc. A 374, 20150294, https://doi.org/10.1098/rsta.2015.0294.

Vance, D., Little, S. H., de Souza, G. F., Khatiwala, S., Lohan, M. C., & Middag, R., 2017. Silicon and zinc biogeochemical cycles coupled through the Southern Ocean. Nature Geoscience, 10(3), 202–206.

Weber, T., John, S., Tagliabue, A., & DeVries, T., 2018. Biological uptake and reversible scavenging of zinc in the global ocean. *Science*, 361(6397), 72–76.

Figure captions

Figure 1. Palaeogeographical reconstruction at 90 Ma with approximate study locations, modified from Jarvis et al. (2011).

Figure 2. Cenomanian–Turonian δ^{114}Cd and δ^{66}Zn stratigraphy of the S57 core from the Tarfaya Basin compared with a) δ^{13}C data from Tsikos et al., 2004, (b) TOC data from Kolonic et al., 2005, and (c) δ^{98}Mo and Mo_{EF} data from Dickson et al., 2016. The chemostratigraphic divisions are as follows: (Division 1) In white are samples from stratigraphically below the onset level of the carbon-isotope excursion that demarcates OAE 2, as well as those from above the termination of the so-called plateau phase that is characterized by the highest carbon-isotope values (c.f. Tsikos et al., 2004). These samples represent background conditions for the Cenomanian–Turonian interval. (Division 2) In dark grey are samples from an interval approximately coeval with the Plenus Cold Event. The timing of this event, initially recognized by the occurrence of boreal fauna and relatively heavy bulk oxygen-isotope compositions in the English chalk, can be correlated to sections that lack characteristic fossils by carbon-isotope chemo-stratigraphy (Gale and Christensen, 1996; Jenkyns et al., 2017; Gale et al., 2019; Gangl

et al., 2019). Here, this chemostratigraphic division is extended just beyond the slight dip in the carbon-isotope curve to cover the interval of relatively lower Cd, Mo, and Zn enrichment factors. (Division 3) In light grey are samples from the intervals that record maximum organic-carbon burial globally during the peak of OAE 2. This division covers a short interval stratigraphically just below sediments recording the Plenus Cold Event and sediments from the overlying plateau phase of the carbon-isotope excursion (c.f. Tsikos et al., 2004).

Figure 3. Cd/Mo and Co × Mn values for the Tarfaya Basin sediments compared to values for modern organic-rich sediments from various environments following Sweere et al. (2016). The shading represents the different chemostratigraphic divisions as highlighted in Figure 2.

Figure 4. δ^{114}Cd and δ^{66}Zn *versus* $\mathrm{Mo_{EF}}$. $\mathrm{Mo_{EF}}$ is used as a proxy for local redox conditions (e.g. Scott and Lyons, 2012). Some outliers of very low δ^{114}Cd and low $\mathrm{Mo_{EF}}$ are attributed to a larger isotopic offset between sediments and seawater in more oxygenated conditions. Patterns for the remaining data imply that local redox conditions were not the dominant control on δ^{114}Cd and δ^{66}Zn.

Figure 5. Close-up of an interval from the S57 core comparing δ^{114}Cd and δ^{66}Zn values with high-resolution $\mathrm{Fe_{py}/Fe_{HR}}$ and Mo isotope and concentration data. Samples marked in red highlight intervals that are taken to reflect a larger isotopic offset between sediments and seawater in more oxygenated conditions. See text for discussion. a) Tsikos et al., 2004, (b) Poulton et al., 2015 (c) Goldberg et al., 2016. The grey-shaded bands reflect anoxic non-sulfidic intervals (Poulton et al., 2015).

Figure 6. Cd and Zn concentrations *versus* Total Organic Carbon (TOC). The shading in (A) reflects the chemostratigraphic divisions as defined in Figure 2. The colours in (B) indicate different ranges of Mo_{EF} values, a proxy for local redox conditions (e.g. Scott and Lyons, 2012).

Figure 7. Comparison of data from organic-rich sediments (this study) and the organic-lean English Chalk at Eastbourne (Sweere et al., 2018) during the Cenomanian–Turonian boundary interval. The two sites are correlated using key points in the C-isotope stratigraphy (Tsikos et al., 2004), as indicated by the dashed lines. The grey-shaded bands highlight time-equivalent intervals of lower $\delta^{66}Zn$.

Figure 8. Simplified global isotopic mass-balance model based on steady-state conditions for different $\delta^{66}Zn_{inputs}$ values. f_{oxic} reflects Zn burial in Fe-Mn phases in oxic conditions (e.g. Little et al., 2014), f_{anoxic} refers to the Zn burial in organic-rich sediments on continental margins (Little et al., 2016), and $f_{euxinic}$ reflects the burial of Zn in strongly euxinic (restricted) basins, like the modern Black Sea (Vance et al., 2016; Isson et al., 2018). The horizontal black line represents modern ocean conditions, the red and blue lines +0.25 and -0.4‰ changes in $\delta^{66}Zn_{seawater}$, as constrained in section 4.4, for the OAE 2 carbon-isotope plateau phase and PCE conditions, respectively. The isotopic offsets between different sedimentary archives and seawater used here are based on observations in the modern ocean as summarized in Vance et al. (2016) and are as follows: $\Delta^{66}Zn_{oxic\text{-}sw} = +0.4$ ‰, $\Delta^{66}Zn_{anox\text{-}sw} = -0.5$ ‰, $\Delta^{66}Zn_{eux\text{-}sw} = 0.0$ ‰. *The estimate for the proportion of f_{eux} relative to f_{anox} comes from output flux estimates by Isson et al. (2018).

Figure 9. Comparison of Cd and Zn data generated in this study. The concentrations show very similar patterns, whereas the δ^{114}Cd and δ^{66}Zn are considerably different. This observation implies that δ^{114}Cd and δ^{66}Zn values provide complementary information on the proportion of oxic sinks and sedimentary and hydrothermal inputs.

Figure 1

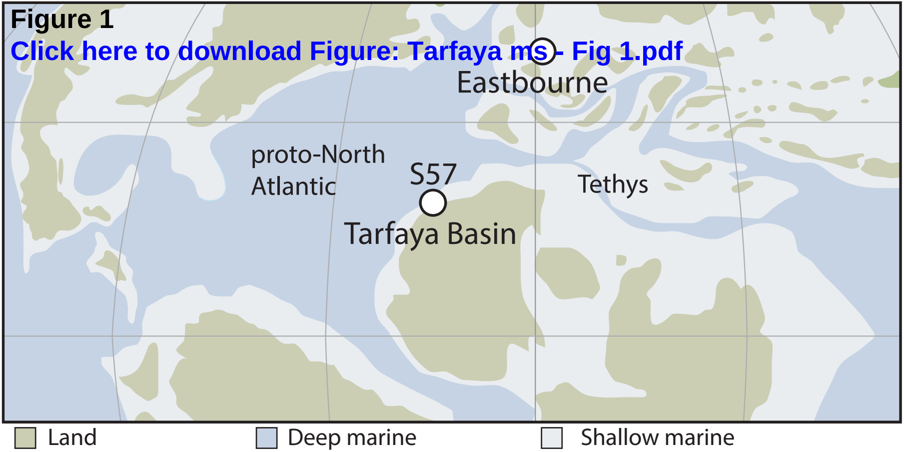
Eastbourne
proto-North Atlantic
S57
Tethys
Tarfaya Basin
Land
Deep marine
Shallow marine

Figure 2


Tarfaya S-57
Depth [m]
δ13Corg [‰] (a)
-30 -28 -26 -24
δ66Zn [‰]
-0.4 0.0 0.4 0.8
δ114Cd [‰]
-0.5 -0.1 0.3
δ98Mo [‰] (c)
-0.2 0.2 0.6 1.0 1.4
Depth [m]
25 30 35 40 45 50 55 60
Turonian
Cenomanian
OAE 2
PCE
1
3
2
1
0 5 10 15 20 25
TOC [%] (b)
1 10 100
Zn [EF]
10 100 1000
Cd [EF]
10 100 1000
Mo [EF] (c)

Figure 3

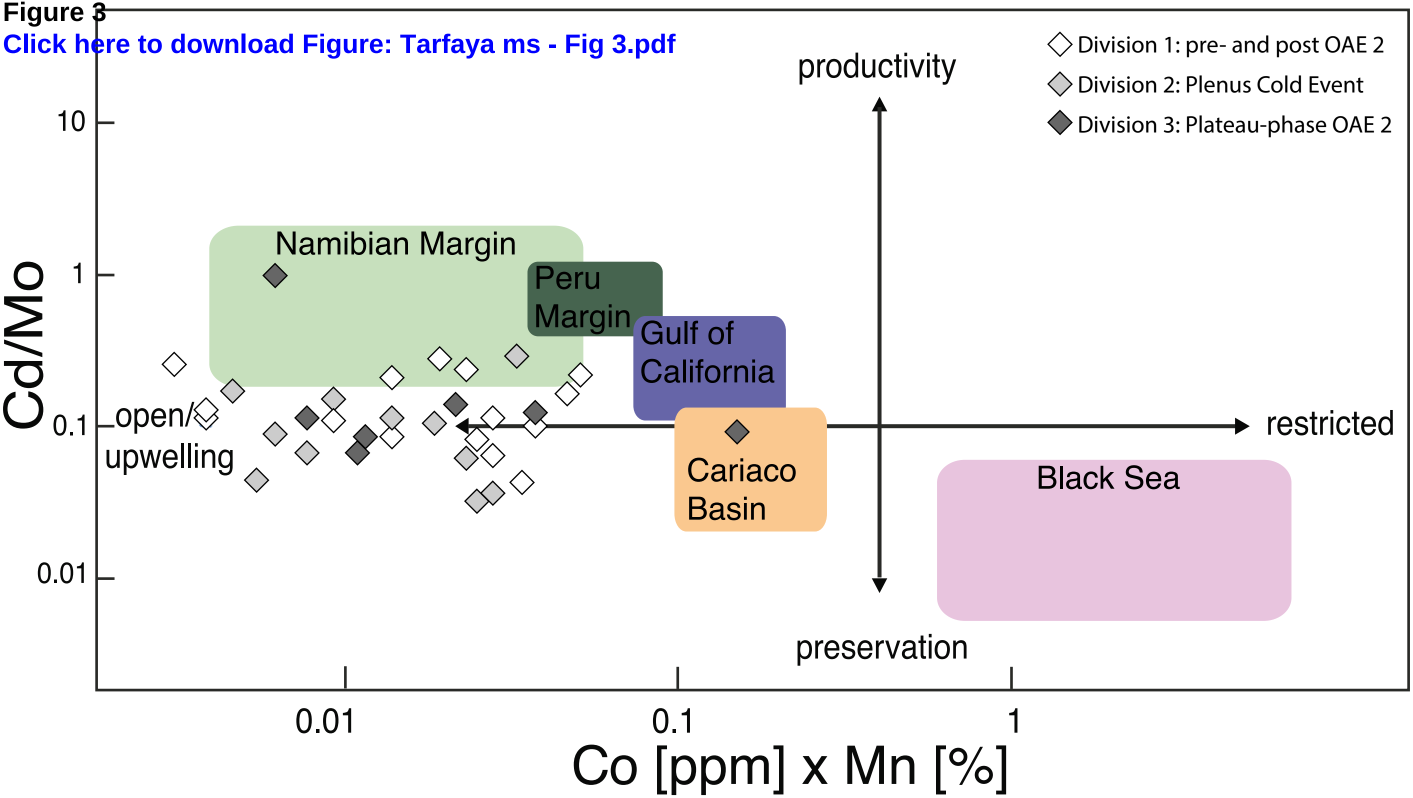

◇ Division 1: pre- and post OAE 2
◇ Division 2: Plenus Cold Event
◆ Division 3: Plateau-phase OAE 2
productivity
preservation
restricted
open/
upwelling
Namibian Margin
Peru Margin
Gulf of California
Cariaco Basin
Black Sea
Cd/Mo
10
1
0.1
0.01
Co [ppm] x Mn [%]
0.01
0.1
1

Figure 4

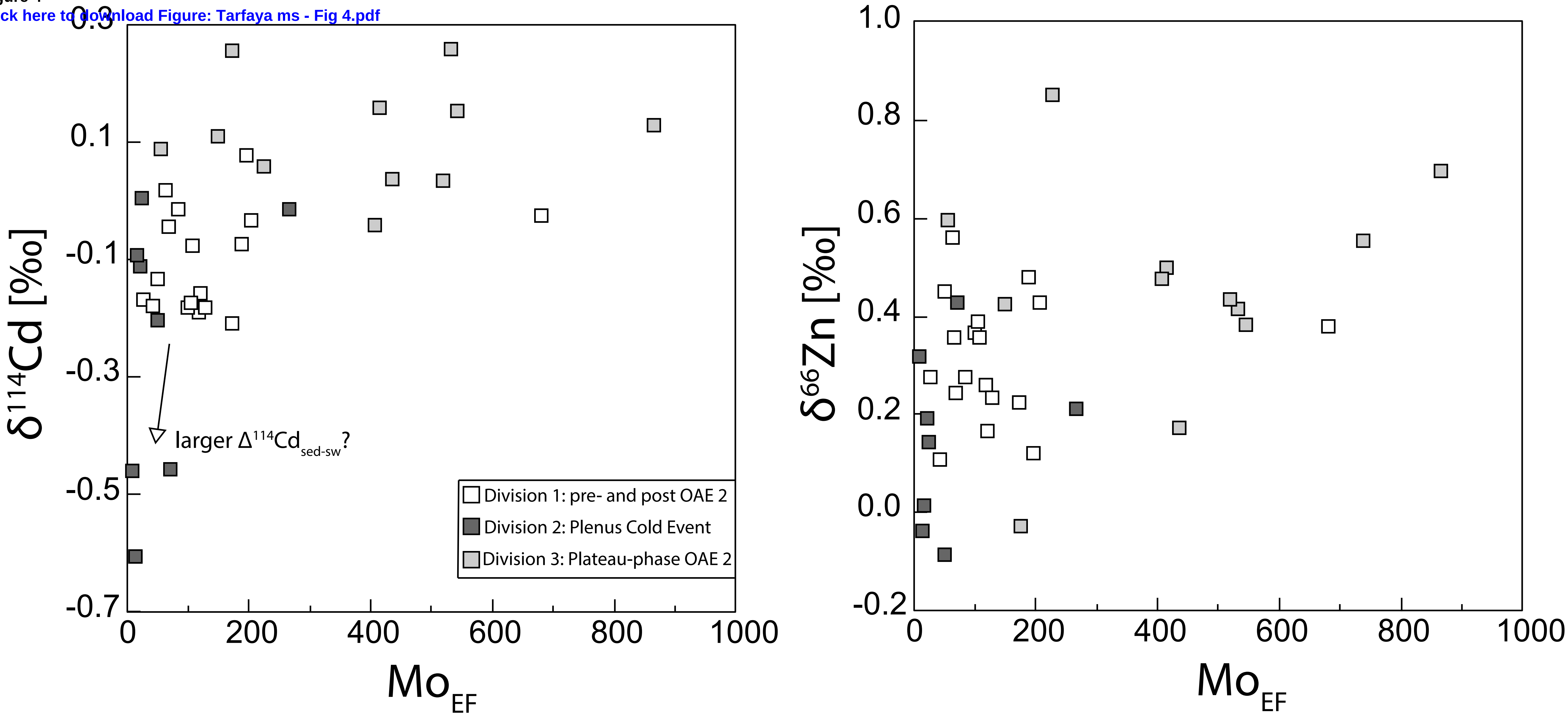
0.3
0.1
-0.1
-0.3
-0.5
-0.7
δ114Cd [‰]
larger Δ114Cd sed-sw?
Division 1: pre- and post OAE 2
Division 2: Plenus Cold Event
Division 3: Plateau-phase OAE 2
0
200
400
600
800
1000
MoEF
1.0
0.8
0.6
0.4
0.2
0.0
-0.2
δ66Zn [‰]
0
200
400
600
800
1000
MoEF

Figure 5

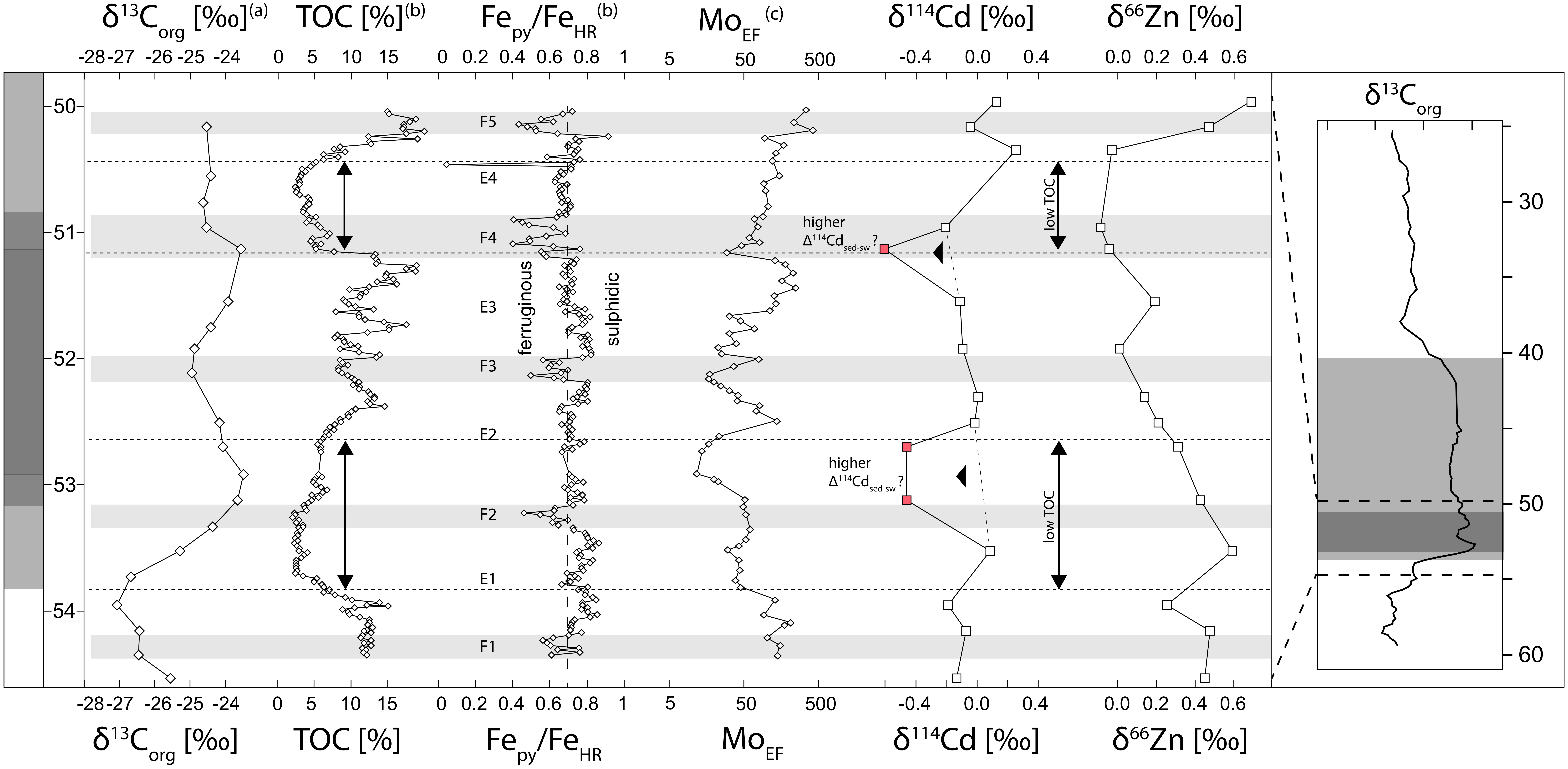
δ13Corg [‰](a)
TOC [%](b)
Fepy/FeHR (b)
MoEF (c)
δ114Cd [‰]
δ66Zn [‰]
-28 -27 -26 -25 -24
0 5 10 15
0 0.2 0.4 0.6 0.8 1
5 50 500
-0.4 0.0 0.4
0.0 0.2 0.4 0.6
-50
-51
-52
-53
-54
F5
E4
F4
E3
F3
E2
F2
E1
F1
ferruginous
sulphidic
higher Δ114Cdsed-sw ?
higher Δ114Cdsed-sw ?
low TOC
low TOC
δ13Corg
30
40
50
60

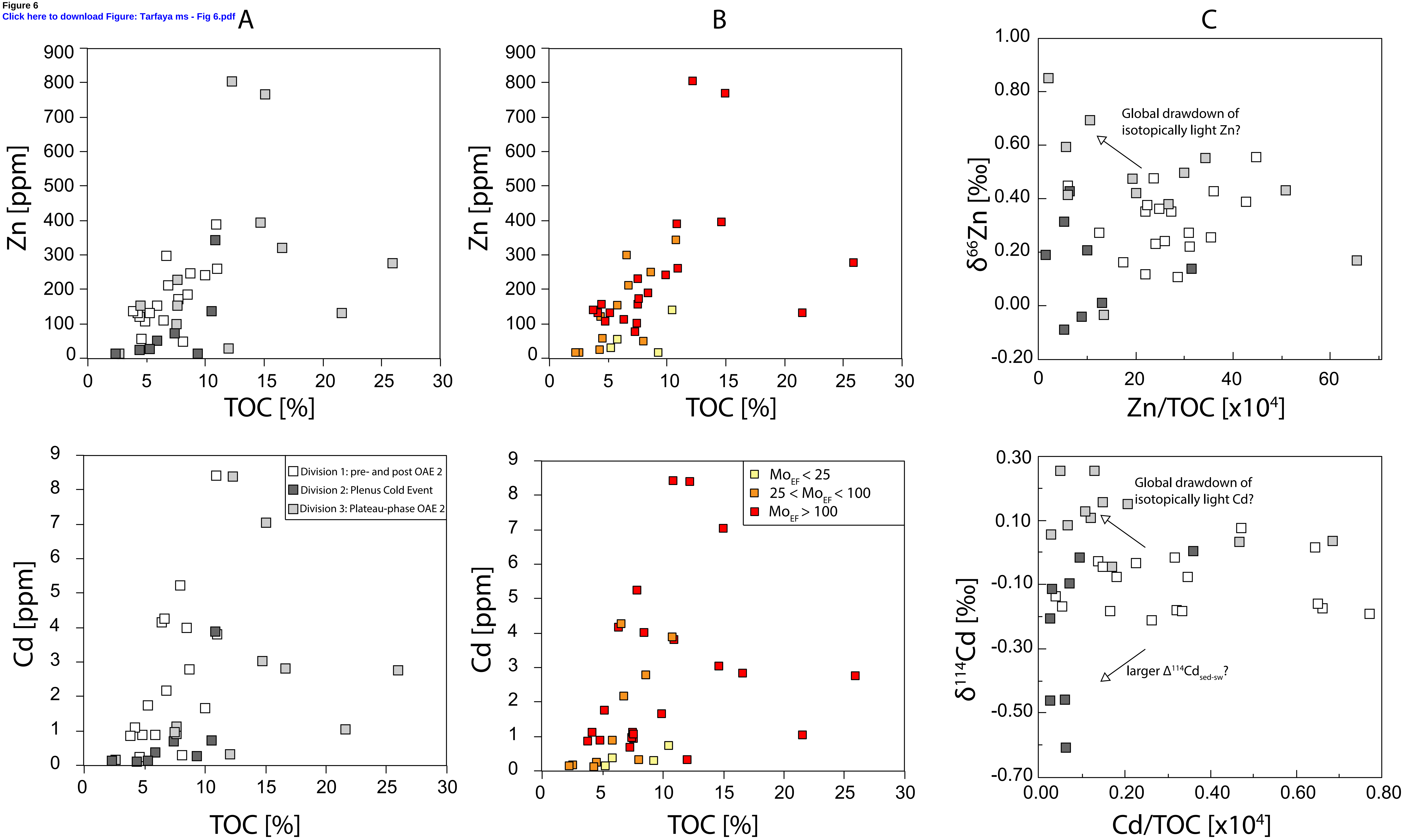
A
B
C
Zn [ppm]
900
800
700
600
500
400
300
200
100
0
TOC [%]
0
5
10
15
20
25
30
δ^{66}Zn [‰]
1.00
0.80
0.60
0.40
0.20
0.00
-0.20
Zn/TOC [x10^{4}]
0
20
40
60
Global drawdown of isotopically light Zn?
Cd [ppm]
9
8
7
6
5
4
3
2
1
0
☐ Division 1: pre- and post OAE 2
■ Division 2: Plenus Cold Event
▨ Division 3: Plateau-phase OAE 2
🟨 Mo$_{EF}$ < 25
🟧 25 < Mo$_{EF}$ < 100
🟥 Mo$_{EF}$ > 100
δ^{114}Cd [‰]
0.30
0.10
-0.10
-0.30
-0.50
-0.70
Cd/TOC [x10^{4}]
0.00
0.20
0.40
0.60
0.80
Global drawdown of isotopically light Cd?
larger Δ^{114}Cd$_{sed-sw}$?

Figure 7

Click here to download Figure: Tarfaya ms - Fig 7.pdf

Figure 8

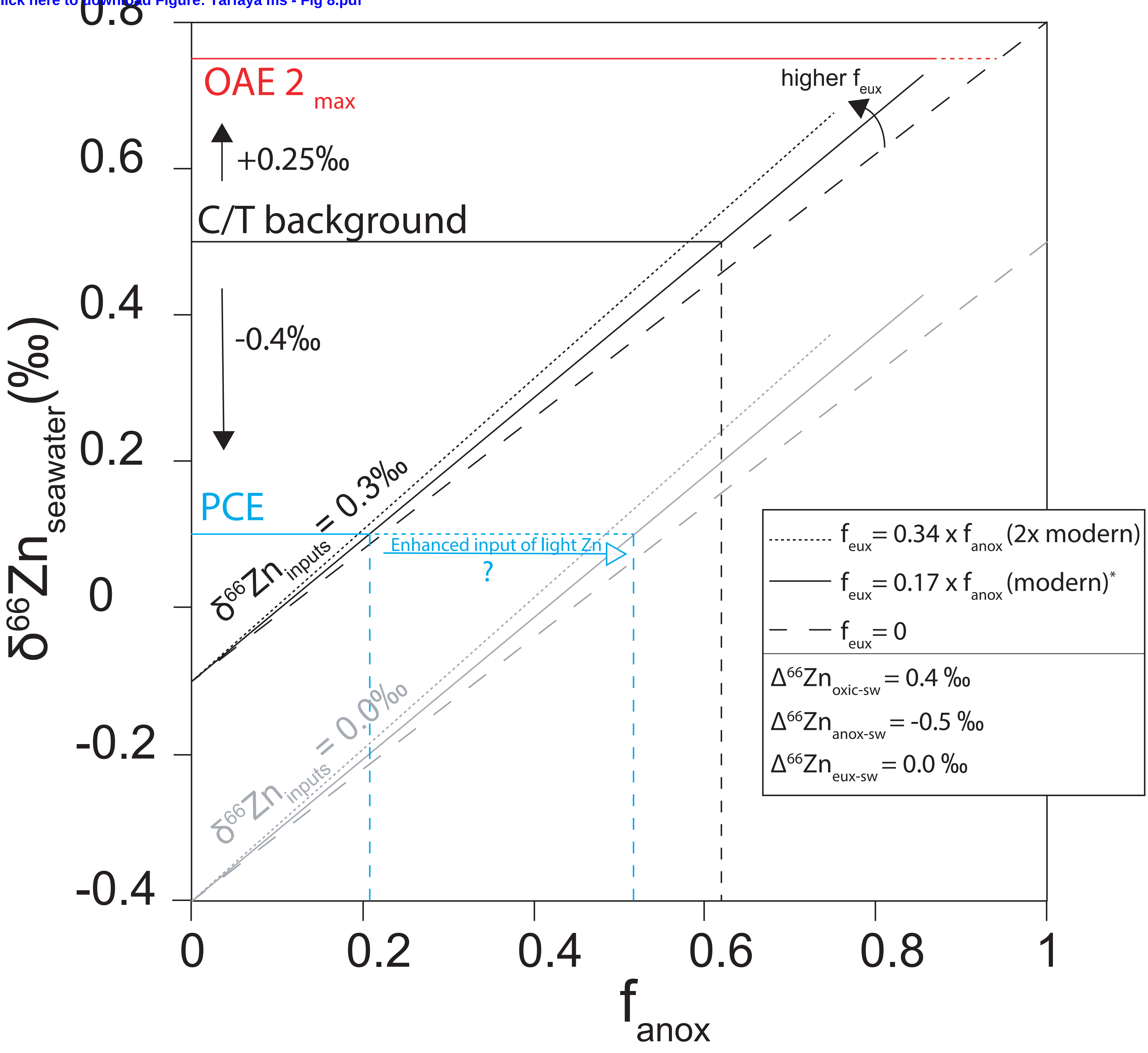
0.8
0.6
0.4
0.2
0
-0.2
-0.4
δ66Znseawater (‰)
0
0.2
0.4
0.6
0.8
1
fanox
OAE 2 max
+0.25‰
C/T background
-0.4‰
PCE
higher feux
δ66Zninputs = 0.3‰
δ66Zninputs = 0.0‰
Enhanced input of light Zn
?
feux = 0.34 x fanox (2x modern)
feux = 0.17 x fanox (modern)*
feux = 0
Δ66Znoxic-sw = 0.4 ‰
Δ66Znanox-sw = -0.5 ‰
Δ66Zneux-sw = 0.0 ‰

Figure 9

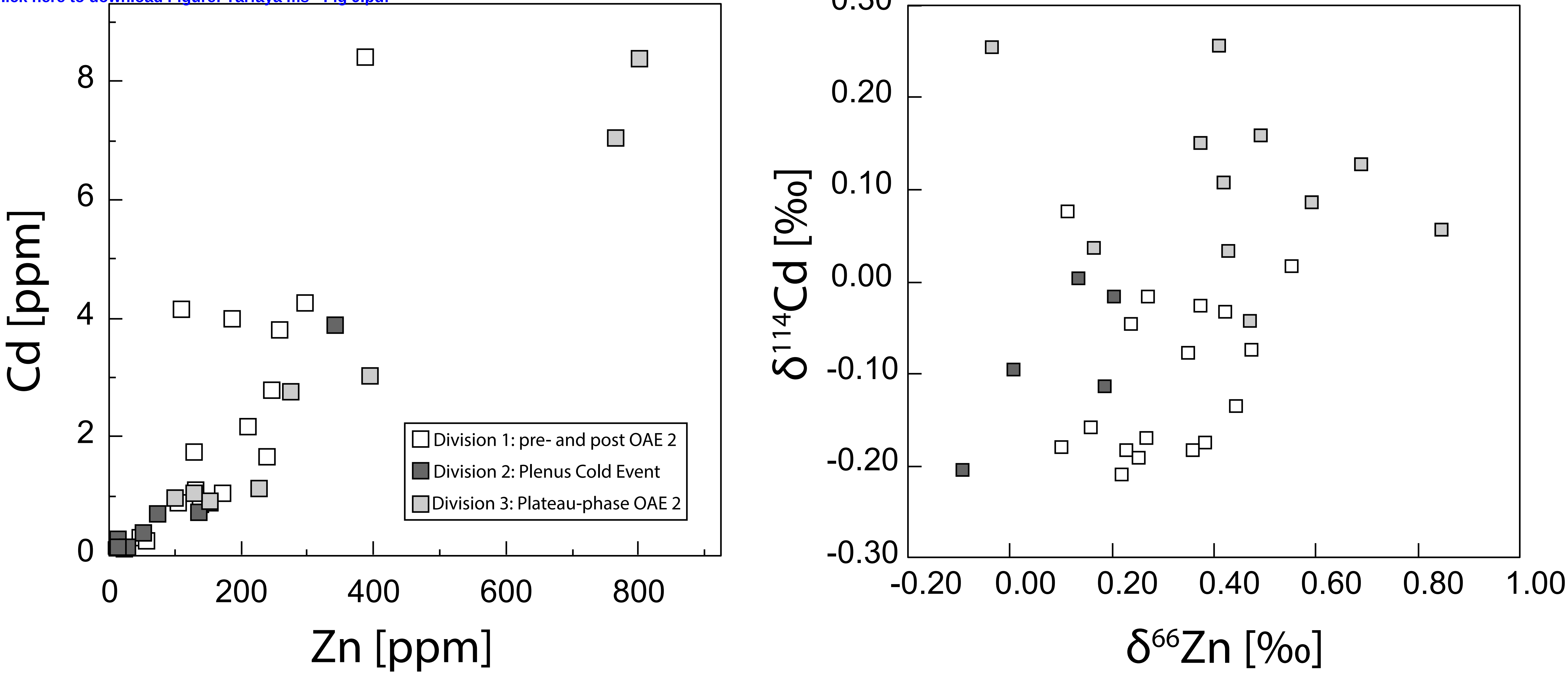
Cd [ppm]
0
2
4
6
8
0
200
400
600
800
Zn [ppm]
☐ Division 1: pre- and post OAE 2
■ Division 2: Plenus Cold Event
▨ Division 3: Plateau-phase OAE 2
0.30
0.20
0.10
0.00
-0.10
-0.20
-0.30
δ^{114}Cd [‰]
-0.20
0.00
0.20
0.40
0.60
0.80
1.00
δ^{66}Zn [‰]